J. Fluid Mech. (2003), *vol.* 482, *pp.* 181–206.
DOI: 10.1017/S0022112003004038 Printed in the United Kingdom

Instability threshold of gaseous detonations

By RÉMI DAOU AND PAUL CLAVIN

Institut de Recherche sur les Phénomènes Hors Équilibre, CNRS/Universités d'Aix-Marseille I & II, 49, rue F. Joliot Curie, BP 146, F-13384 Marseille, cedex 13, France

(Received 13 March 2002 and in revised form 18 July 2002)

The spectrum of linear modes governing the multidimensional instabilities of gaseous detonations is revisited by combining a numerical analysis with new analytical results. In view of recent developments in nonlinear analyses for describing the cellular structure of weakly unstable detonation fronts, particular attention is paid to the neighbourhood of the instability threshold. A first objective is to check the validity domain of the analytical results and to investigate to what extent they are useful when approaching the self-sustained regime (Chapman–Jouguet conditions). A second objective is to study how the multidimensional instabilities are influenced by multiple-step chemistry. The roles of the induction period and of the stiffness of the exothermic runaway will be investigated separately.

1. Introduction

A detonation consists of a strong inert shock followed by a subsonic reacting flow which is described by the reactive Euler equations. The pioneering analysis of Erpenbeck (1964) showed that a planar detonation may be stable when the heat release is sufficiently small. A detailed study of the neighbourhood of the instability onset is a preliminary step in studying the cellular structures by a nonlinear analysis of a weakly unstable detonation. Such a weakly nonlinear analysis consists of a systematic reduction in complexity, taking into account the leading-order nonlinearities near threshold. Does the same reduction continue to be meaningful under real conditions of strongly unstable detonations? No answer can be given with certainty, but understanding of strong instabilities may nevertheless be enhanced by investigating their onset. For example, the weakly nonlinear analysis of Clavin & Denet (2002) predicts time-dependent patterns similar to those observed in experiments. The leading nonlinear mechanisms of a weakly unstable detonation in the multidimensional case are different from those in planar geometry: in a galloping detonation (one-dimensional case) they come from the heat-release rate, see Clavin & He (1996), while they are concerned with the Reynolds stress in the diamond patterns of a cellular detonation, see Clavin & Denet (2002).

Stability limits of detonation waves were first investigated by numerical analyses of the linear spectrum of the problem, see the pioneering work of Erpenbeck (1964, 1965) and the more recent works of Lee & Stewart (1990) and Short & Stewart (1998). The instability of a strongly overdriven wave was explained few years ago by Clavin & He (1996) and Clavin, He & Williams (1997) within the framework of two approximations: a small difference between the specifics heats, $(\gamma - 1) \ll 1$, $\gamma \equiv c_p/c_v$, and a large Mach number of propagation, $\bar{M}_U^2 \gg 1$. The multidimensional instability of a planar wave occurs when the heat release as a fraction of the enthalpy of the post-shock gas (Neumann spike, subscript N) $q \equiv \hat{Q}/c_p\bar{T}_N$, is increased above

a critical value which is as small as the two parameters $(\gamma - 1)$ and $1/\bar{M}_U^2$. By taking all these small parameters to be of same order of magnitude, the neighbourhood of the instability threshold has been described by the linear analysis of Clavin & He (2001). This asymptotic analysis is valid for general irreversible chemistry but is restricted to large overdrive. The simplification comes from the approximation of low Mach number, valid everywhere across the detonation structure (behind the leading shock), leading to a clear distinction between the isobaric gas expansion and the compressibility effects (acoustics), yielding a convenient way to shed light on the physical mechanisms that are competing near threshold.

Ordinary detonations are strongly unstable with a moderate degree of overdrive and thus are outside the domain of validity of the above-mentioned analyses. However, by considering a large density jump across the leading (strong) shock, $\bar{M}_U^2 \gg 1$, occurring at large overdrive near the stability limits, an essential feature of the dynamics of real detonations is taken into account, namely a large deflection of the streamlines across the wrinkled shock. On the other hand, for small overdrive, near Chapman–Jouguet (C-J) conditions, the propagation Mach number of a weakly unstable detonation is close to unity, and the density jump is small. Therefore, when attention is limited to weakly unstable detonations, it is worth considering the limit of a large degree of overdrive.

This paper presents a study of the linear dynamics of detonation waves near threshold for a wide range of overdrive and different chemical kinetics. The objective is to provide a solid background for further nonlinear studies of the diamond patterns of a cellular detonation front. A comparison between numerical and analytical results is presented. The first part of the paper determines to what extent the results of Clavin & He (2001) may be still useful when the quasi-isobaric approximation fails on approaching the C-J regime. The problem is addressed also by comparison with another perturbation analysis by Short & Stewart (1999). In their analysis, which is free from assumptions concerning $(\gamma - 1)$ and $\bar{M}_U^2$, Short & Stewart (1999) used $\hat{Q}/R\bar{T}_N$ as a small parameter together with a one-step Arrhenius model ($\hat{Q}$ is the heat release and $R \equiv (c_p - c_v)$ the gas constant of a perfect gas). They also limit their attention to sufficiently small activation energies so that the rate of heat release is a monotonic function decreasing with the distance from the shock. This model provides a simple framework within which to check the validity domain of a perturbation method based only on a small parameter $\hat{Q}/R\bar{T}_N$.

The asymptotic solution of Clavin & He (2001) is valid for $\hat{Q}/R\bar{T}_N \equiv \gamma q/(\gamma - 1)$ of order unity, as is the case at instability threshold for moderate and small overdrive, as will be seen later, see for example figure 6. Moreover, the analysis is free from assumptions concerning the kinetics of the irreversible heat release. The dynamics of a detonation front being very sensitive to the chemical kinetics, the possibility of investigating any distribution of heat-release rate is particularly convenient for studying real detonations. The second part of the paper is devoted to the effects of multiple-step chemistry near threshold. The influences of the induction delay and of the stiffness of the exothermic runaway (ratio of the runaway time to the induction delay) upon the linear spectrum are investigated in the multidimensional case by a numerical analysis in the light of the analytical results of Clavin & He (2001). This is carried out for a wide range of overdrive within the framework of the three-step chemistry model considered previously by Short & Dold (1996) and later by Sanchez *et al.* (2001). The occurrence of high-frequency modes and short wavelengths at the instability threshold is investigated.

The paper is self-contained and has the following structure. Results of Short & Stewart (1999) and of Clavin & He (2001) are briefly recalled in § 2. An outline of the later analysis is given in Appendix A, where particular attention is paid to the key points ensuring the validity of the results for $\hat{Q}/R\bar{T}_N$ of order unity. An overall physical understanding of the mechanisms competing near threshold is also provided in § 2. A comparison of the two analyses is presented in § 3, where a common domain of validity is exhibited for large overdrive. A systematic comparison with numerical results is provided in § 4 for moderate overdrive. Section 5 is devoted to the effects of multiple-step chemistry. The influences of parameters such as the induction time and the stiffness of the thermal runaway are investigated. A conclusion is given in § 6.

2. Theoretical background

In a one-dimensional unperturbed detonation wave, the flow Mach number $\bar{M}$ (relative to the shock) increases with the heat release from its post-shock value ($\bar{M}_N < 1$) to its value at the end of the chemical reaction ($\bar{M}_B \leqslant 1$), $\bar{M}_N \leqslant \bar{M} \leqslant \bar{M}_B$. At the end of an irreversible reaction, the flow becomes just sonic in a self-sustained detonation (C-J wave), $\bar{M}_{B,CJ} = 1$, while it remains subsonic when the detonation is piston-supported (overdriven waves) $\bar{M}_B < 1$. The degree of overdrive is defined as $f \equiv (\bar{M}_U/\bar{M}_{U,CJ})^2$ where $\bar{M}_U$ is the shock-propagation velocity divided by the sound speed in the initial mixture and $\bar{M}_{U,CJ}$ is the propagation Mach number of the self-sustained wave. The faster the piston is, the larger is $\bar{M}_U$ and the smaller are $\bar{M}_N$ and $\bar{M}_B$. Within a perfect gas approximation, the propagation regime is fully determined by three parameters, namely the specific heats ratio $\gamma = c_p/c_v$, the propagation Mach number $\bar{M}_U$ (or f) and the heat release divided by the post-shock gas enthalpy, $q \equiv \hat{Q}/c_p\bar{T}_N$. The inner structure is controlled by the chemical kinetics. Ordinary detonations are strongly unstable with a moderate degree of overdrive ($f \approx 1$). As a rule, they exhibit a large density jump across the leading shock ($\bar{M}_U^2 \gg 1$); typical density ratios are larger than 6 and may reach 10 in gaseous detonations.

2.1. *Analysis of Clavin & He*

Weakly unstable detonations with a large density jump exist only when $f \gg 1$. These regimes are studied by Clavin & He (2001) within the approximation $(\gamma - 1) \ll 1$ by a perturbation method based on a small parameter ϵ defined as

$$\epsilon^2 \equiv \gamma \bar{M}_N^2 \approx (\gamma - 1)/2 + 1/\bar{M}_U^2 \ll 1 \tag{2.1}$$

(typical values are $\gamma \approx 1.2$–1.3, $\bar{M}_U^2 \approx 30$, $\bar{M}_N^2 \approx 0.15$–0.18). Stability or weak instability then occurs when q is as small as $\gamma - 1$ and $1/\bar{M}_U^2$ and the distinguished limit to be considered is

$$\gamma - 1 = O(\epsilon^2), \quad 1/\bar{M}_U^2 = O(\epsilon^2), \quad q \equiv Q/c_p\bar{T}_N = O(\epsilon^2). \tag{2.2}$$

The previous analysis of Clavin *et al.* (1997) for $q = O(1)$, corresponded to more unstable detonations and did not include conditions near threshold.

Defining the position of the wrinkled shock as $\hat{x} = \hat{\alpha}(\hat{t}, \hat{\boldsymbol{y}})$, with $\hat{t}$ denoting the time and $\hat{x}$ and $\hat{\boldsymbol{y}}$ the longitudinal and the transverse coordinates, we introduce the non-dimensional coordinates $\xi \equiv \int_{\hat{\alpha}}^{\hat{x}} \hat{\rho}(\hat{x}', \hat{t})\,\mathrm{d}\hat{x}'/(\bar{\rho}_N\bar{d})$ (the shocked gases are in the region $\xi > 0$), $\boldsymbol{\eta} \equiv \epsilon\hat{\boldsymbol{y}}/\bar{d}$ and $\tau \equiv \hat{t}/\bar{t}_N$, where $\hat{\rho}$ is the density, $\bar{t}_N$ is the post-shock reaction time defining the transit time of a fluid particle across the detonation

structure, and $\bar{d}$ is the detonation width, $\bar{d} \equiv \bar{u}_N \bar{t}_N$, $\bar{u}_N$ being the post-shock flow velocity relative to the shock. Scaling of the transverse coordinates is dictated by the range of unstable wave-lengths, $\hat{\lambda} \approx \bar{d}/\epsilon$, resulting from a resonance between the neutral modes of the leading shock (with a frequency $\hat{\omega} \approx 2\pi\bar{a}_N/\hat{\lambda}$, where $\bar{a}_N$ is the sound speed in the compressed gas, see D'yakov 1954 and Kontorovich 1957) and the oscillatory instability of the shock–reaction complex (frequency $\hat{\omega} \approx 1/\bar{t}_N$, see Clavin *et al.* (1997)). In the linear approximation $\varphi(\xi, \boldsymbol{\eta}, \tau) = \bar{\varphi}(\xi) + \delta\varphi(\xi, \boldsymbol{\eta}, \tau)$, where $\delta\varphi$ denotes the perturbation, and in a Fourier representation, $\alpha(\boldsymbol{\eta}, \tau) = \alpha^* \exp(s\tau + \mathrm{i}\boldsymbol{\kappa}\cdot\boldsymbol{\eta})$, $\delta\varphi = \delta\varphi^*(\xi)\exp(s\tau + \mathrm{i}\boldsymbol{\kappa}\cdot\boldsymbol{\eta})$, where superscript * denotes Fourier components and where the complex growth rate $\hat{\sigma}$ and the transverse wave vector $\hat{\boldsymbol{k}}$ have been reduced according to

$$s = \hat{\sigma}\bar{t}_N, \qquad \boldsymbol{\kappa} = \frac{\hat{\boldsymbol{k}}\bar{d}}{\epsilon}; \tag{2.3}$$

the eigenvalue $s(\kappa)$ is obtained in the limit (2.2) in the form of an expansion

$$s(\kappa) = s_0(\kappa) + \epsilon^2 s_2(\kappa) + O(\epsilon^4). \tag{2.4}$$

The leading-order solution $s_0(\kappa)$ corresponds to the oscillatory modes of the inert shock, $q = 0$, and is fully controlled by the isobaric entropy–vorticity wave, yielding

$$\frac{\partial^2}{\partial\tau^2}\alpha - \nabla^2\alpha = 0 \Rightarrow s_0(\kappa) = \pm\mathrm{i}\kappa, \tag{2.5}$$

with $\kappa \equiv |\boldsymbol{\kappa}|$, see equations (A 10) and (A 11) in Appendix A. The growth (or damping) rate $\mathrm{Re}(s)$ is small compared to the oscillatory frequency $\mathrm{Im}(s)$, (2.5), and is obtained at the following order of the perturbation analysis by imposing a boundedness condition at infinity (in the burned gas) to the sound waves. The result may be written in a compact form as

$$\frac{1}{q}\mathrm{Re}[s(\kappa)] = \tfrac{1}{2}\mathrm{Re}[s_0 Z(s_0)] - \frac{\kappa}{Q}\sqrt{1 + \frac{2}{(\gamma-1)\bar{M}_U^2}}\left|\mathrm{Im}\sqrt{1 + Q[Z(s_0) - 1]}\right|, \tag{2.6}$$

where $(\gamma-1)\bar{M}_U^2$ and Q are parameters of order unity characterizing the propagation regime of the unperturbed solution,

$$Q \equiv \frac{2q}{(\gamma-1)} = \frac{2}{\gamma}\frac{\hat{Q}}{R\bar{T}_N} = O(1), \tag{2.7}$$

see Clavin & He (2001) and Appendix A. The influence of the chemical kinetics appears through the function $Z(s_0)$ which is defined by

$$Z(s_0) \equiv \int_0^\infty \bar{w}'_{\bar{M}_U}(\xi)\exp(-s_0\xi)\,\mathrm{d}\xi + \int_0^\infty (1 + s_0\xi)\bar{w}(\xi)\exp(-s_0\xi)\,\mathrm{d}\xi, \tag{2.8}$$

where, according to (2.5), $s_0 = \pm\mathrm{i}\kappa$. The function $\bar{w}(\xi)$, $\int_0^\infty \bar{w}(\xi)\,\mathrm{d}\xi = 1$, is the non-dimensional distribution of heat-release rate across the unperturbed wave, and $\bar{w}'_{\bar{M}_U}(\xi)$, $\int_0^\infty \bar{w}'_{\bar{M}_U}(\xi)\,\mathrm{d}\xi = 0$, describes its modification when varying the propagation Mach number $\bar{M}_U$, $\epsilon^2\delta\bar{w}(\xi) = \bar{w}'_{\bar{M}_U}(\xi)\delta\bar{M}_U/\bar{M}_U$ ($\bar{w}'_{\bar{M}_U}(\xi) = \beta(\gamma-1)w'_\theta(\xi)$ in the notation of Clavin *et al.* 1997 and Clavin & He 2001). The scaling $\bar{w}'_{\bar{M}_U}(\xi) = O(1)$ is convenint near threshold in the limit (2.2): the sensitivity of the chemical reaction rate does not influence the stability limits when the order of magnitude of $\max|\bar{w}'_{\bar{M}_U}(\xi)|$ is smaller than unity, and the detonation is always strongly unstable when it is larger.

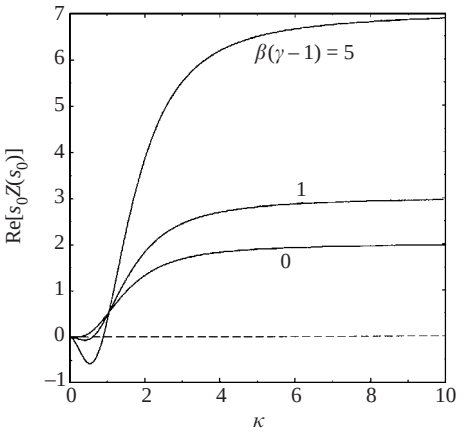

FIGURE 1. $\mathrm{Re}[s_0 Z(s_0)]$ vs. κ for an Arrhenius law with $\beta q = 0.1$ and $\beta(\gamma-1) = 0$, 1 and 5.

The quasi-isobaric gas expansion due to heat release being clearly distinguished from the compressible effects, the oscillatory instability of the shock–reaction complex is illuminated by the quasi-isobaric approximation resulting from (2.2), as briefly explained now; see also the discussion below equation (A 24) in Appendix A.

(i) The isobaric gas expansion is responsible for the instability and is represented by the first term on the right-hand side of (2.6), see figure 1. The flow Mach number being small, the leading-order modifications to gas density are due to variations in heat-release rate and propagate from the inert shock to the burned gases with the entropy–vorticity wave. The derivative with respect to time of the total post-shock mass of gas has to be balanced by the mass flux across the shock. When expressed in the original variables (ξ, η, τ), this yields an integral equation for the velocity of the perturbed shock, describing the ocillatory instability, see Clavin & He (2001) and Clavin & Denet (2002).

(ii) The sound waves triggered in the burned gases have a smaller amplitude than the entropy–vorticity wave by a factor ϵ^2, see equation (A 13) in Appendix A. Although the pressure variations have a negligible effect upon the energy equation, sound waves nevertheless produce a negative feedback upon the isobaric combustion instability through a velocity coupling (see the discussion below equation (A 24) in Appendix A). This acoustic feedback which is described by the second term on the right-hand side of (2.6) (negative contribution to $\mathrm{Re}[s(\kappa)]$) is essential in multidimensional geometry to damp out the disturbances with small transverse wavelengths which would be amplified by the quasi-isobaric instability as shown in figure 1. We will come back to this point a few lines below.

(iii) In one-dimensional geometry the instability, called galloping detonation, results from the sensitivity of the heat-release-rate distribution $|\bar{w}'_{\bar{M}_U}(\xi)| \neq 0$, see Clavin & He (1996). The situation is different in multidimensional geometry. The deflection of the streamlines across the wrinkled shock perturbs the heat-release-rate distribution and excites an oscillatory instability even in the absence of chemical sensitivity, $|\bar{w}'_{\bar{M}_U}(\xi)| = 0$, see Clavin *et al.* (1997). A detonation which is stable to longitudinal disturbances may then be unstable to multidimensional disturbances. In the following, we will denote as 'hydrodynamic instability' the instability of a detonation wave which develops when $|\bar{w}'_{\bar{M}_U}(\xi)| = 0$ (no chemical kinetics effects) so that $Z(s_0)$ reduces to the second term on the right-hand side of (2.8).

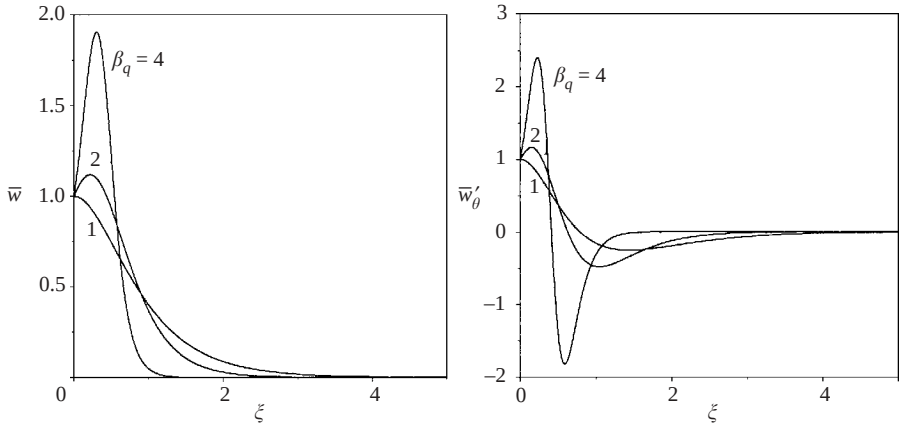

FIGURE 2. Profiles of $\bar{w}(\xi)$ and $\bar{w}'_\theta(\xi)$ for an Arrhenius law with $q = 1$ and $\beta q = 1$, 2 and 4.

To summarize, equation (2.6) describes a competition between a destabilizing mechanism, the gas expansion due to a quasi-isobaric heat release (first term), and a damping one due to compressible effects (second term). The existence of a bifurcation is easily shown from (2.6) by noticing that, for small Q, $Q \ll 1$, the damping term dominates whatever the wavelength,

$$\frac{2}{q}\mathrm{Re}[s(\kappa)] \to \mathrm{Re}[s_0 Z(s_0)] - \sqrt{1 + \frac{2}{(\gamma-1)\bar{M}_U^2}}\,|\mathrm{Re}[s_0 Z(s_0)]| < 0, \tag{2.9}$$

and the planar front is stable. In the opposite limit, $Q \gg 1$, the acoustic term is negligible (except at small wavelengths, see below) and the planar detonation is unstable to transverse disturbances with $\kappa = O(1)$. In any case, thanks to the sound waves, the detonation is stable to disturbances with a small wavelength, $\kappa \gg 1$ (the second term on the right-hand side of (2.6) is proportional to $-\kappa$ in the limit $\kappa \to \infty$ while $Z(s_0) \to 0$ and $\mathrm{Re}[s_0 Z(s_0)] \to$ positive constant, see figure 1).

Equation (2.6) is valid for a general irreversible chemistry. For comparison with the results of Short & Stewart (1999), a one-step chemical reaction controlled by an Arrhenius law is considered in §§ 3 and 4. In this simple case, the kinetics is characterized by a single parameter, the reduced activation energy $\beta \equiv E/RT_N$. Within the quasi-isobaric approximation, the distributions $\bar{w}(\xi)$ and $\bar{w}'_{\bar{M}_U}(\xi)$ are given by the solution of the equation $\bar{w}(\xi) = \mathrm{d}\bar{Y}/\mathrm{d}\xi = (1-\bar{Y})\exp(\beta q \bar{Y})$ with $\bar{Y} = 0$ at $\xi = 0$ where $\bar{Y}$ is the mass fraction of the products, giving $\bar{w}'_{\bar{M}_U}(\xi) = \beta(\gamma-1)w'_\theta(\xi)$ where $w'_\theta(\xi) \equiv \mathrm{d}(\xi\bar{w})/\mathrm{d}\xi$ (see Clavin & He 1996 and Clavin *et al.* 1997). The β parameter then appears in (2.8) through two quantities, $\beta(\gamma-1)$ and βq. According to (2.7), $Q = 2\beta q/\beta(\gamma-1)$, and the right-hand side of (2.6) is fully determined by three non-dimensional parameters of order unity: $(\gamma-1)\bar{M}_U^2$, βq (or Q) and $\beta(\gamma-1)$. Large values of the reduced activation energy may be retained in the limit (2.2) when $\beta q = O(1)$. The double limit $\beta \to \infty$ and $q \to 0$ is essential to avoid singularities appearing for an infinitely large activation energy; see the discussion in Clavin *et al.* (1997). The parameter βq controls the shape of the distributions $\bar{w}(\xi)$ and $w'_\theta(\xi)$ ($\int_0^\infty \bar{w}(\xi)\,\mathrm{d}\xi = 1$, $\int_0^\infty \bar{w}'_\theta(\xi)\,\mathrm{d}\xi = 0$), see figure 2, while $\beta(\gamma-1)$ measures the intensity of the thermal sensitivity. The quasi-isobaric instability is exhibited by the curve $\mathrm{Re}[\pm\mathrm{i}\kappa Z(\pm\mathrm{i}\kappa)]$ vs. κ ($s_0 = \pm\mathrm{i}\kappa$) and typical examples are

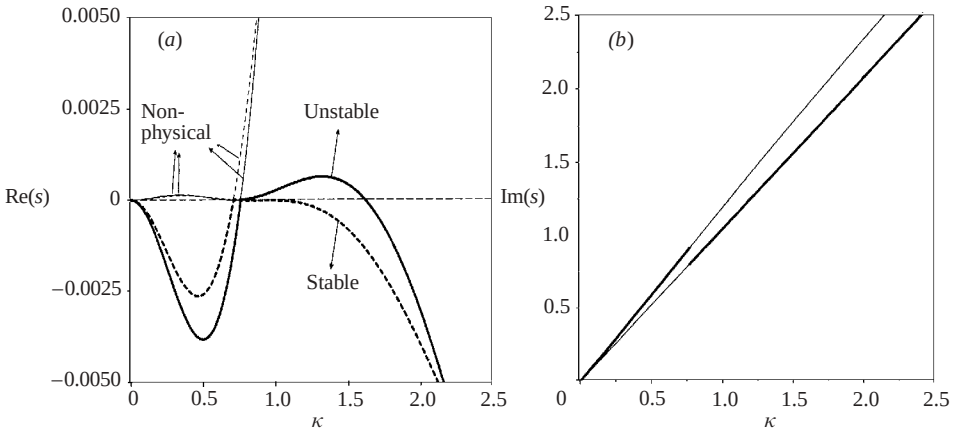

FIGURE 3. (*a*) Growth rates Re(s) vs. κ given by equation (2.6) with $(\gamma - 1) = 0.1$, $\beta = 10$ and $M_U^2 = 50$ for an unstable case $q = 0.04$ (bold solid line) and a stable one $q = 0.03$ (bold dashed line). (Non-physical parts are plotted as thin lines.) (*b*) Frequency, Im(s) vs. κ, for the unstable case (bold solid line) of (*a*).

given in figure 1 for $\beta q = 0.1$ and for different values of $\beta(\gamma - 1)$. In the particular case investigated by Short & Stewart (1999), $\beta q \ll 1$, the reaction rate becomes a monotonic function, decreasing with distance from the shock; $\bar{w}(\xi) = \exp(-\xi)$ when $\beta q = 0$. When $\beta(\gamma - 1) \ll 1$, the heat-release distribution does not vary much when the propagation regime is changed, the effects of the chemical sensitivity become negligible, $\bar{w}'_{\bar{M}_U}(\xi) \approx 0$, and we are dealing with a pure 'hydrodynamic instability'.

An example of a dispersion relation near onset of the instability as obtained from (2.6) with an Arrhenius law is shown in figure 3. The expression Re$[s(\kappa)]$ given by (2.6) results from two roots of a quadratic equation when only the branches of solutions that satisfy a boundedness condition of the acoustic waves in the burned gas ($\xi \to +\infty$) are retained. The result is plotted in bold (solid or dashed) lines in figure 3 and corresponds to two pieces of two different branches (the negative part of Re$[s(\kappa)]$ at small κ belongs to a different branch than the rest of the curve). The non-physical part of the branches is plotted as thin lines. It is worth noticing for the following (see § 5) that even in the stable case, the intersection of the two branches leads to the existence of a marginally stable mode, Re$(s) = 0$, $\kappa \neq 0$. A simplification occurs in the case of 'hydrodynamic instability' considered in § 4, $\beta(\gamma - 1) \ll 1$; the first term on the right-hand side of (2.8) becoming negligible, $\bar{w}'_{\bar{M}_U}(\xi) \approx 0$, one has Re$[s_0 Z(s_0)] > 0$ at every κ (see figure 1). Equation (2.6) then corresponds to the same branch of solution in the entire κ domain $[0, \infty]$ (see figures 9*a*, *b*, 11*a*, *b* and 13*a*, *b*).

2.2. *Analysis of Short & Stewart*

Within the framework of an Ahrrenius model with $\beta q \ll 1$ and using a non-dimensional wave vector $\boldsymbol{k}$ and growth rate σ reduced, respectively, by the half-reaction length $\bar{d}_{1/2}$ and the half-reaction time, $\bar{t}_{1/2} \equiv d_{1/2}/\bar{a}_N$,

$$\sigma = \hat{\sigma}\bar{t}_{1/2}, \qquad \boldsymbol{k} = \hat{\boldsymbol{k}}\bar{d}_{1/2}, \tag{2.10}$$

the dispersion relation obtained by the perturbation analysis of Short & Stewart (1999) for a small heat release, without any assumption concerning $(\gamma - 1)$ or M_U^2,

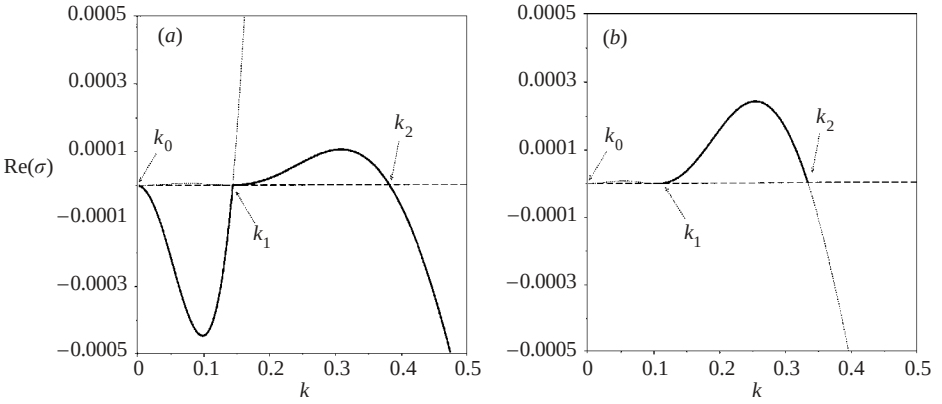

FIGURE 4. Growth rate $\mathrm{Re}(\sigma)$ vs. k result obtained with (a) equation (2.6) and (b) equation (2.11) for $\gamma = 1.4$, $\beta = 1$, $q = 0.1$ and $M_U^2 = 50$.

can be written as

$$\frac{1}{q}\mathrm{Re}(\sigma) = \frac{\gamma^3(\gamma+1)(\gamma(\gamma+1))^{1/2}}{4\sqrt{2}}\frac{1}{2}C\,\mathrm{Re}(\Sigma), \tag{2.11}$$

where C is given by

$$C \equiv \left[-\frac{2}{\gamma(\gamma-1)M_U^2}\left(\frac{2}{\gamma(\gamma+1)}\right)^{1/2} + \frac{2\sqrt{2}(\gamma-1)Q}{(\gamma+1)(\gamma(\gamma+1))^{1/2}} \pm \frac{Q}{k}\mathrm{Im}(\Sigma)\right],$$

where Σ is a complex function of $k \equiv |\boldsymbol{k}|$, involving the parameters γ and $\beta(\gamma-1)$, which is explicitly given in equations (8.35)–(8.36) of Short & Stewart (1999).

By comparison with equation (2.6), equation (2.11) explicitly involves the parameter γ in addition to $(\gamma-1)\bar{M}_U^2$, $\beta(\gamma-1)$ and Q, but it contains only linear terms in Q. A preliminary comparison of the two dispersion relations is shown in figure 4 for an unstable case with $\gamma = 1.4$. The parts of the solution corresponding to $\mathrm{Re}(\sigma) > 0$ look qualitatively similar. No part with $\mathrm{Re}(\sigma) < 0$ appears in the results of Short & Stewart because such parts correspond to incoming acoustic waves. These authors retain only outgoing waves, while Clavin & He retain all the solutions with sound waves (incoming or outgoing) bounded in the limit ($\xi \to +\infty$). A systematic comparison is carried out in the two next sections.

3. Theoretical results for large overdrive

The stability limits Q versus $(\gamma-1)\bar{M}_U^2$ and the critical wavelength $\lambda_c \equiv 2\pi/\kappa_c$ obtained from the theoretical results (2.6) and (2.11) for a detonation sustained by an Arrhenius law are plotted in figure 5 for $(\gamma-1)\beta = 5$, in figure 6 for $(\gamma-1)\beta = 1$ and in figure 7 for $(\gamma-1)\beta = 0$. When expressed in terms of Q and $(\gamma-1)\bar{M}_U^2$ the results given by (2.6) are independent of γ, while those obtained from (2.11) and/or from numerics depend slightly on γ in the range $\gamma = 1.05$–1.2. In figure 5, the values of the activation energy ($\beta = 100$ and $\beta = 25$) are higher than assumed in the analysis of Short & Stewart (1999). This is not the case in figures 6 ($\beta = 5$) and 7 ($\beta = 0$). However, equation (2.11) is still meaningful at very strong overdrive for the stability limits in figure 5, because both βq and Q become sufficiently small. According to the stability limits of figures 5 to 7, the critical value of Q decreases on

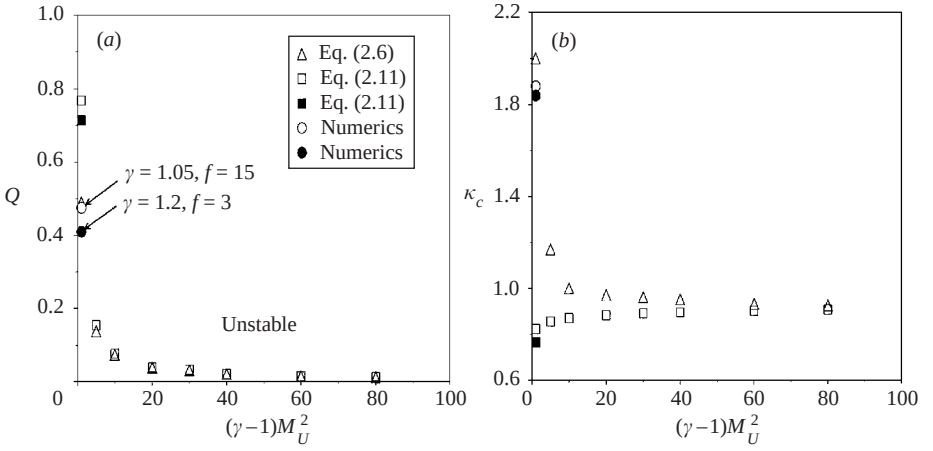

FIGURE 5. (*a*) Stability limits Q vs. $(\gamma-1)\bar{M}_U^2$, and (*b*) critical wavenumber κ_c vs. $(\gamma-1)\bar{M}_U^2$, obtained for $(\gamma-1)\beta = 5$ from (2.6) (white triangles) and from (2.11) with $\gamma = 1.05$ (white squares). The results obtained from (2.11) with $\gamma = 1.2$ are similar, as shown by the black square for the particular value $(\gamma-1)\bar{M}_U^2 = 1$. For comparison, numerical results are presented for $\gamma = 1.2$ (black circles) and $\gamma = 1.05$ (white circles).

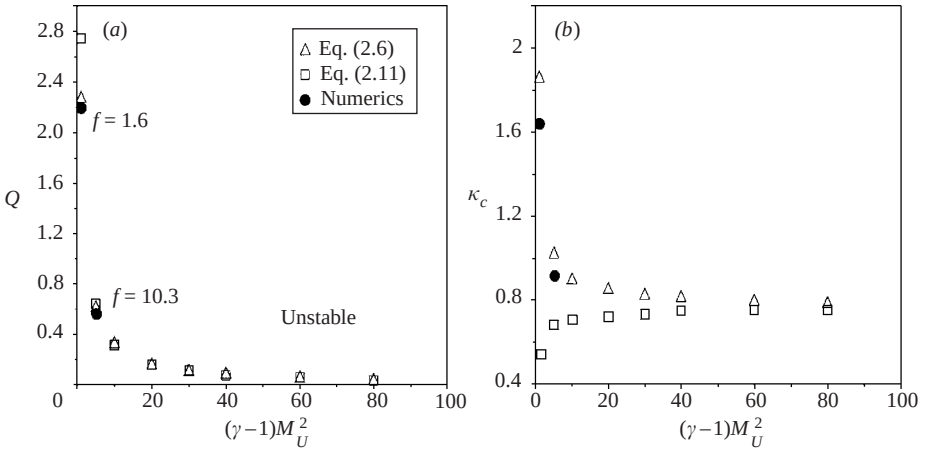

FIGURE 6. (*a*) Stability limits Q vs. $(\gamma-1)\bar{M}_U^2$, and (*b*) critical wavenumber κ_c vs. $(\gamma-1)\bar{M}_U^2$, obtained for $(\gamma-1)\beta = 1$ from (2.6) (white triangles) and from (2.11) with $\gamma = 1.2$ (white squares). For comparison, numerical results are presented for $\gamma = 1.2$ (black circles).

increasing $(\gamma-1)\bar{M}_U^2$ (increasing the overdrive factor f). This is true whatever the activation energy β and the ratio of specific heats γ.

By construction of both analyses, one may expect that equation (2.6) for an Arrhenius law in the double limit $\beta q \ll 1$ and $Q \ll 1$ yields the same result as equation (2.11) in the double limit $(\gamma-1) \ll 1$ and $f \gg 1$. A good agreement between the two approaches is effectively observed in figures 5 and 7 for $Q \ll 1$ and/or $(\gamma-1)\bar{M}_U^2 \gg 1$, corresponding to $f \gg 1$. This may be seen directly from the analytical expressions (2.6) and (2.11) as follows:

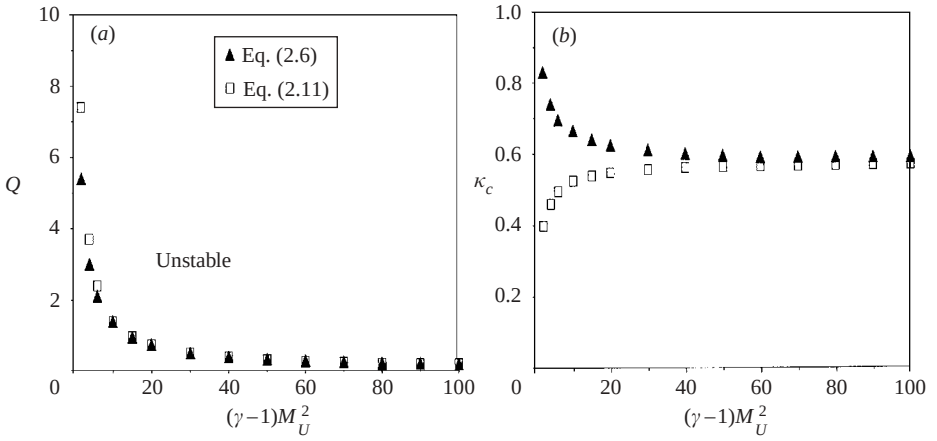

FIGURE 7. (*a*) Stability limits Q vs. $(\gamma-1)\bar{M}_U^2$ and (*b*) critical wavenumber κ_c vs. $(\gamma-1)\bar{M}_U^2$ obtained with $(\gamma-1)\beta=0$ from (2.6) (triangles) and from (2.11) for $\gamma=1.05$ (squares).

(i) In the limit $\beta q \ll 1$, $(\gamma-1)\beta = O(1)$, we have $\bar{w}(\xi)=\exp(-\xi)$, and the integrals in (2.8) can be easily computed, yielding

$$Z(s_0) \approx \frac{1+s_0[2+(\gamma-1)\beta]}{(1+s_0)^2}. \tag{3.1}$$

When (3.1) is introduced into (2.6), and when only the terms linear in Q and in $1/(\gamma-1)M_U^2$ are retained, a result is obtained which looks similar to (2.11),

$$\frac{1}{q}\mathrm{Re}(s) \approx \frac{\kappa^2}{[1+\kappa^2]^2}\Bigg[-\frac{\kappa^2}{(\gamma-1)\bar{M}_U^2} - \frac{Q}{2}\frac{\kappa^4(\kappa^2-1)}{[1+\kappa^2]^2} - \tfrac{1}{2}(\gamma-1)\beta\left\{\frac{Q}{2}\frac{\kappa^2}{[1+\kappa^2]^2}(1-6\kappa^2+\kappa^4)+\frac{\kappa^2-1}{(\gamma-1)\bar{M}_U^2}\right\} - \tfrac{1}{2}(\gamma-1)^2\beta^2 Q\frac{\kappa^2(1-\kappa^2)}{[1+\kappa^2]^2}\Bigg], \tag{3.2}$$

valid when $(\gamma-1)\ll 1$ with

$$(\gamma-1)\bar{M}_U^2 \gg 1, \qquad Q \equiv \frac{2q}{(\gamma-1)} \ll 1, \qquad (\gamma-1)\beta = O(1), \tag{3.3}$$

implying $\beta q \ll 1$. Notice that the result takes an even simpler form when $(\gamma-1)\beta$ becomes negligibly small (pure hydrodynamic instability): The stability limit Q versus $(\gamma-1)\bar{M}_U^2$ predicted by (3.2) reduces to a hyperbola, $Q(\gamma-1)\bar{M}_U^2=16$, with a critical wavenumber $\kappa_c* \to 1/\sqrt{3}$ when $(\gamma-1)\bar{M}_U^2 \to \infty$, in agreement with the results in figure 7.

(ii) On the other hand, in the limit $(\gamma-1)\ll 1$, $(\gamma-1)\bar{M}_U^2 \gg 1$ and $(\gamma-1)\beta = O(1)$, the expressions for $\mathrm{Re}(\Sigma)$ and $\mathrm{Im}(\Sigma)$ in (2.11) reduce to

$$\mathrm{Re}(\Sigma) = 2\epsilon\ln(2)\frac{\kappa^2}{(\kappa^2+1)^2}\left[\kappa^2+\tfrac{1}{2}(\kappa^2-1)(\gamma-1)\beta\right] + (\text{h.o.t.}), \tag{3.4}$$

$$\frac{1}{k}\mathrm{Im}(\Sigma) = \pm\frac{\kappa^2}{(\kappa^2+1)^2}[1-\kappa^2+2(\gamma-1)\beta] + (\text{h.o.t.}), \tag{3.5}$$

where the time and length scales used by Short & Stewart (1999) have been expressed in terms of the scales of Clavin & He (2001) in the form $\sigma = \bar{M}_N \ln(2) s + (\text{h.o.t.})$ and $k = \sqrt{\gamma}\bar{M}_N \ln(2)\kappa + (\text{h.o.t.})$, see Appendix B. When (3.4) and (3.5) are introduced into the dispersion relation (2.11), equation (3.2) is recovered.

To summarize, considering detonations controlled by a one-step Arrhenius law, the two results (2.6) and (2.12) are equivalent near threshold when $(\gamma - 1) \ll 1$, $f \gg 1$ and $\beta q \ll 1$, corresponding to the range of parameters (3.3) describing overdriven detonations with a distribution of heat-release rate decreasing monotonically with the distance from the shock. However, according to figures 5 to 7, discrepancies appear near threshold for moderate overdrive (when decreasing $(\gamma - 1)\bar{M}_U^2$ i.e. decreasing f), where Q is no longer small.

None of the analyses of Short & Stewart (1999) (valid for small Q) and of Clavin & He (2001) (valid for large f) seem very appropriate for $f \approx 1$. How accurate is equation (2.6), and how much do the results differ from the exact solution for $f \approx 1$? This question, which is addressed in the next section by a comparison with numerical results, is of importance for the rest of the paper when studying multiple-step chemistry.

4. Hydrodynamic instability

The numerical analysis of the linear spectrum at the instability threshold is revisited in this section using the same shooting method as Short & Stewart (1998), see Appendix C. We limit here our attention to the same model as Short & Stewart (1999), an Arrhenius law with $\beta q \ll 1$. The objective is to provide a better insight into the linear dynamics near threshold by carrying out a comparison of the numerical results with (2.6) and (2.11) and by investigating conditions for small and moderate overdrive, outside the validity domains of the theoretical analyses. In order to further simplify the presentation and to emphasize the essential features, it is sufficient to consider the simplest case of a pure hydrodynamic instability $\beta(\gamma - 1) \ll 1$. As indicated by the numerical results plotted in figures 5 and 6, the conclusions are similar for $(\gamma - 1)\beta$ of order unity.

One is thus lead to investigate in more detail the case $\beta = 0$. The problem is now fully determined by three parameters, γ, $\bar{M}_U$ and Q. The numerical results for the stability limits are plotted in a diagram of Q versus $(\gamma - 1)\bar{M}_U^2$ for different values of γ: $\gamma = 1.05$ in figure 8(a), $\gamma = 1.2$ in figure 10(a) and $\gamma = 1.4$ in figure 12(a). The numbers shown in these figures are the overdrive degree f. The critical wavenumber $\kappa_c \equiv 2\pi/\lambda_c$ (λ_c is the critical wavelength) at the bifurcation is plotted in figures 8(b), 10(b) and 12(b) for $\gamma = 1.05, 1.2, 1.4$, respectively. Stability limits and κ_c obtained from (2.6) and (2.11), previously plotted in figure 7(a, b) for $\gamma = 1.05$, are compared with numerical results in figures 8(a, b), 10(a, b) and 12(a, b) for different γ. Numerical results concerning the variation of the growth rate with the wavelength, $\mathrm{Re}[s(\kappa)]$, are plotted in comparison with (2.6) and (2.11) in figures 9(a, b), 11(a, b) and 13(a, b) for typical values of the parameters. The discussion may be summarized as follows:

(i) Let us first discuss the cases $(\gamma - 1) \ll 1$. The stability limit and κ_c given by (2.6) show excellent agreement with the numerical results when $\gamma = 1.05$ and $(\gamma - 1)\bar{M}_U^2 > 5$ ($f > 32$), see figure 8(a, b). Figure 9(a) illustrates that equation (2.6) is an asymptotic result in the limit (2.2). The accuracy deteriorates for $(\gamma - 1)\bar{M}_U^2 \leqslant 1$, but it is still satisfactory when $(\gamma - 1)\bar{M}_U^2 = 1$ ($f \approx 6$), where Q becomes as large as 10, as shown in figure 9(b). For example, when $(\gamma - 1)\bar{M}_U^2 = 1$, the bifurcation is obtained at $Q = 10.4$ ($f = 6$) with the numerical analysis and at $Q = 9.6$ with (2.6)

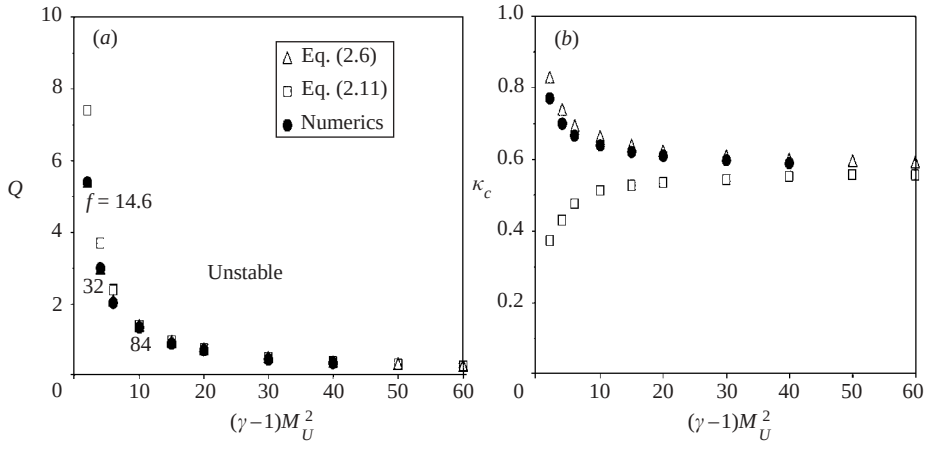

FIGURE 8. (*a*) Stability limit and (*b*) critical wavenumber κ_c given by (2.6) (triangles), by (2.11) (squares) and by the numerical solution (circles) for $\beta = 0$ and $\gamma = 1.05$. The overdrive degree f at threshold is also given with the numerical results.

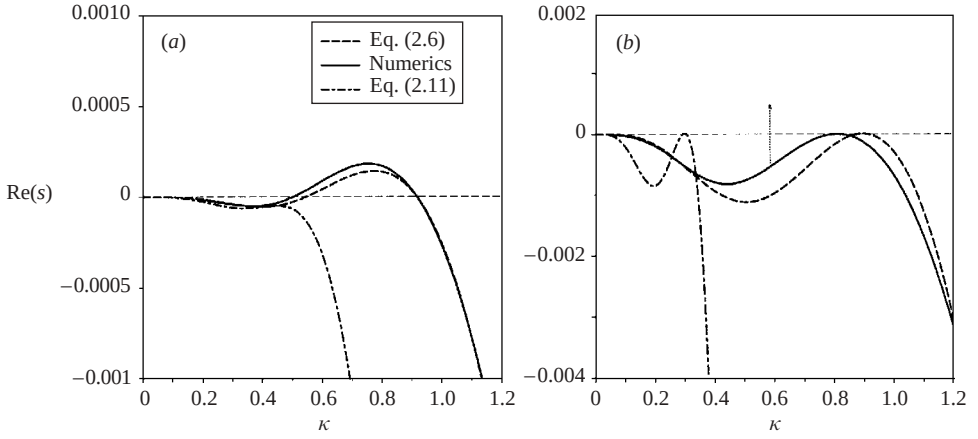

FIGURE 9. (*a*) Comparison of the growth rate vs. κ given by (2.6) (dashed line), (2.11) (dashed-doted line) and by the numerical results (solid line) for $\beta = 0$, $\gamma = 1.05$, $(\gamma-1)\bar{M}_U^2 = 5$ and $Q = 2.8$ ($q = 0.07$, $f = 38$). (*b*) Growth rate vs. κ at threshold for $(\gamma-1)\bar{M}_U^2 = 1$ and $\gamma = 1.05$. The numerical results correspond to $Q = 10.4$ ($f = 6$) and are plotted as a solid line. Equation (2.6) corresponds to $Q = 9.6$ and is plotted as a dashed line. Equation (2.11) corresponds to $Q = 15$ and is plotted as a dashed-dotted line.

and the two functions $\mathrm{Re}[s(\kappa)]$ are quite similar near threshold. The accuracy of (2.6) is satisfactory down to $f = 3$. The results $\mathrm{Re}[s(\kappa)]$ obtained with (2.11) are accurate at very large overdrive, but they are no longer accurate even for an overdrive degree as large as $f = 38$, see figure 9(*a*), and discrepancies become worse when f decreases further, see figure 9(*a*, *b*). This is because Q becomes too large.

(ii) Let us now consider a more realistic case with a larger value of $(\gamma - 1)$. The situation for $\gamma = 1.2$ is presented in figures 10(*a*, *b*) and 11(*a*, *b*). Numerical results have been obtained down to $f = 1.5$. They are in full agreement with the pioneering results of Erpenbeck (1964, 1965), obtained between $f = 1.05$ and $f = 3$. Comparison with the analytical results (2.6) and (2.11) leads to conclusions similar to those of the

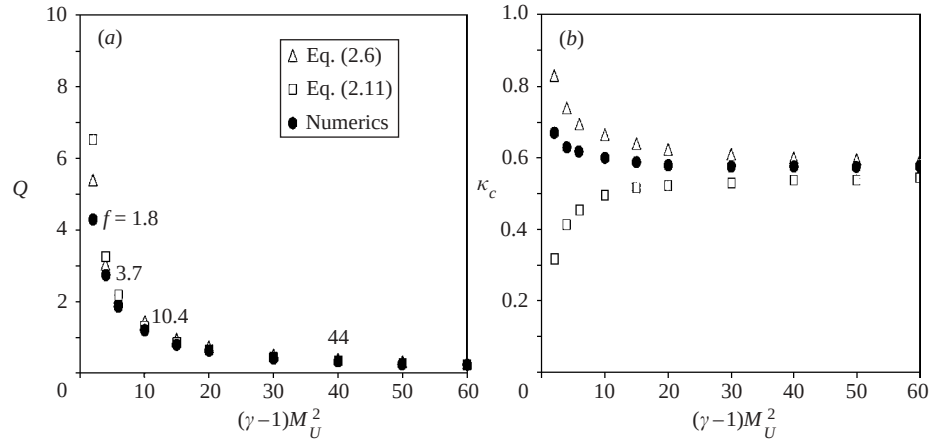

FIGURE 10. (*a*) Stability limit and (*b*) critical wavenumber κ_c given by (2.6) (triangles), (2.11) (squares) and by the numerical results (circles) for $\beta = 0$ and $\gamma = 1.2$.

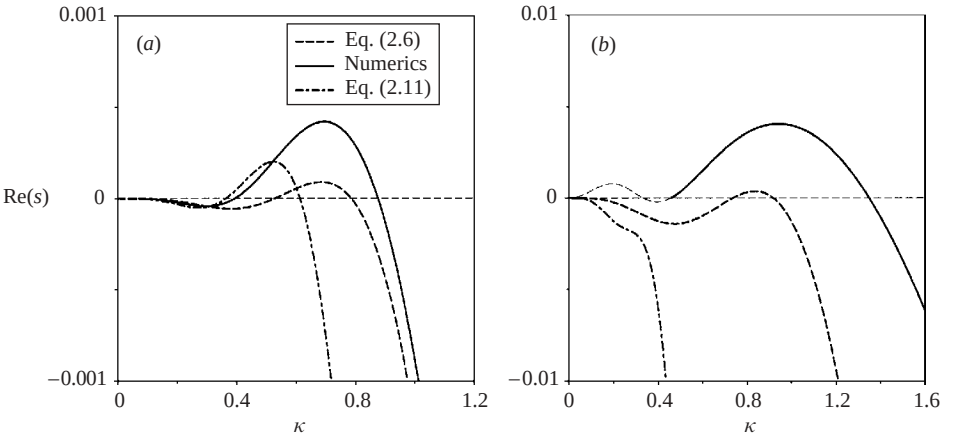

FIGURE 11. Growth rate vs. κ given by (2.6) (dashed line), (2.11) (dashed-dotted line) and by the numerical calculations (solid line) for $\beta = 0$, $\gamma = 1.2$ and (*a*) $(\gamma-1)\bar{M}_U^2 = 10$, $Q = 1.5$ ($q = 0.15$, $f = 8.7$), and (*b*) $(\gamma-1)\bar{M}_U^2 = 2$, $Q = 5.5$ ($q = 0.55$, $f = 1.5$).

preceding case. However, for the same degree of overdrive, the critical value of Q at the instability threshold is smaller than in the case $\gamma = 1.05$ ($f \approx 2$ corresponds to $Q \approx 4$ when $\gamma = 1.2$ and to $Q > 10$ when $\gamma = 1.05$), and the result (2.11) is better than in the preceding case, see figure 11(*a*) for $f = 8.7$. The accuracy of (2.6) is not as good as in the previous case $\gamma = 1.05$, but the stability limits and the critical wavelength at moderate overdrive are still predicted with a better accuracy by (2.6) than by (2.11), see figure 10(*a*, *b*) for $f < 10$ ($(\gamma-1)\bar{M}_U^2 < 10$).

(iii) For $\gamma = 1.4$, the situation is somehow different. The critical value of Q is smaller than unity when $f > 3$, and the linear dynamics near threshold is now more accurately represented by (2.11) than by (2.6) when $f > 6$, $(\gamma-1)\bar{M}_U^2 > 15$, see figure 13(*a*). But none of the results are accurate for $f < 3$, see figure 13(*b*), and the critical wavelength is still better predicted by (2.6) than by (2.11), see figure 12(*b*).

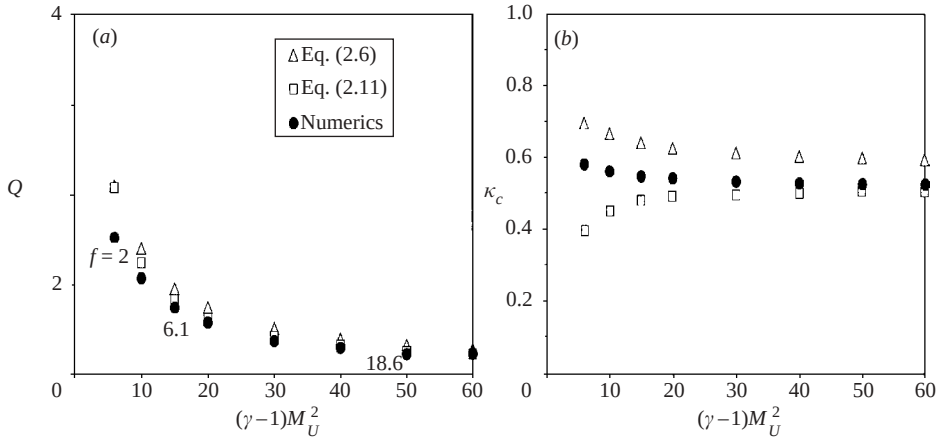

FIGURE 12. (*a*) Stability limit and (*b*) critical wavenumber κ_c given by (2.6) (triangles), (2.11) (squares) and by the numerical results (circles) for $(\gamma-1)\beta=0$ and $\gamma=1.4$.

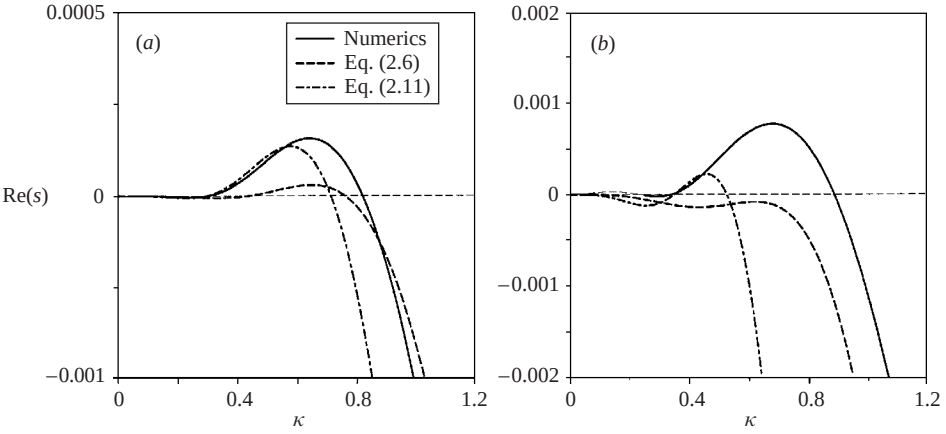

FIGURE 13. Growth rate vs. κ given by (2.6) (dashed line), (2.11) (dashed-dotted line) and by the numerical calculations (solid line) for $\beta=0$, $\gamma=1.4$ and (*a*) $(\gamma-1)\bar{M}_U^2=40$, $Q=0.45$ ($q=0.09$, $f=9.3$) and (*b*) $(\gamma-1)\bar{M}_U^2=10$, $Q=1.35$ ($q=0.27$, $f=2.6$).

To summarize, the distinguished limit (2.2) is convenient for describing the linear dynamics close to the stability limits for large overdrive and when $\gamma\leqslant 1.3$. The results for moderate overdrive are more accurate when obtained by the distinguished limit (2.2) than by a perturbation analysis using Q as a small parameter. Since the critical value of Q at the instability threshold increases with decreasing f, the compressibility effects cannot be captured well by the first term of a small-Q expansion, which is only valid for large overdrive. The sound waves are more accurately described (whatever be Q) by a second-order approximation in the distinguished limit (2.2), see equation (A 24) in Appendix A. However, near C-J regimes, the compressibility effects become dominant and cannot be taken into account accurately, neither by (2.6) nor by (2.11). This is also the case with an Arrhenius model in the presence of destabilizing chemical kinetics, $\beta(\gamma-1)\neq 0$, leading to $Q<1$ near threshold, see figure 14. In this figure, a critical case is presented for $\gamma=1.4$, $\beta(\gamma-1)=5$ and $f=1.2$ which, according to the numerical results, corresponds to conditions at

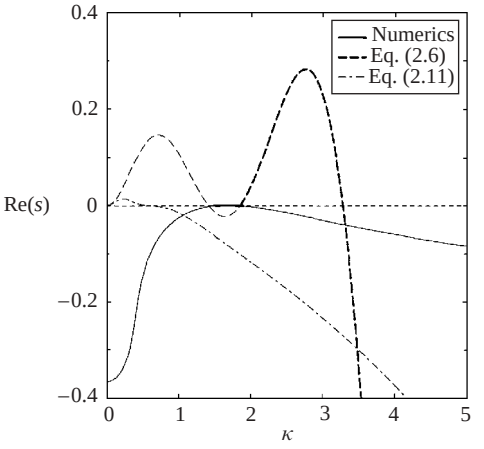

FIGURE 14. Growth rates vs. κ for $(\gamma-1)\beta = 5$, $(\gamma-1)\bar{M}_U^2 = 1.12$ and $Q = 0.55$ ($f = 1.2$).

the instability threshold, $(\gamma-1)\bar{M}_U^2 = 1.12$ and $Q = 0.55$. Equation (2.11) predicts a critical wavelength which is too large by a factor two, while (2.6) predicts that the wave is unstable with a wavelength of the most amplified disturbance smaller by a factor $2/3$ than the critical wavelength. It is noteworthy that the branch of the numerical solution $\mathrm{Re}(s(\kappa))$ that bifurcates differs qualitatively from the analytical solution (2.6). The branch leaves the origin $\kappa = 0$ from a stable oscillatory mode of the one-dimensional case, $\mathrm{Re}(s) < 0$, $\mathrm{Im}(s) \neq 0$. This is no longer a 'hydrodynamic branch' leaving the origin $\kappa = 0$, $s = 0$. As shown by a recent study of Clavin & Williams (2002) in one-dimensional geometry, detonations near threshold and near the C-J regime ($f \approx 1$) require a different theoretical approach, taking into account a quasi-transonic character of the flow throughout the detonation structure. However, as explained in the introduction, weakly unstable detonations for strong overdrive could be more relevant for describing real detonations than weakly unstable C-J waves.

5. Chain-branching kinetics

Various aspects of complex chemistry have a strong influence upon the detonation cellular structure and may be investigated near threshold in the limit (2.2) with equation (2.6). The linear spectrum is complex and involves a variety of branches of solution, $\sigma(\kappa)$. The analytical result (2.6) serves as a helpful guide for carrying out a numerical study, including conditions near self-sustained regimes, $f \approx 1$. The problem is addressed here within the framework of the three-step model used previously by Short & Dold (1996) and Sanchez *et al.* (2001):

initiation	:	$F \longrightarrow R$	$k_I = A_I \exp(-\beta_I/T)$,
chain-branching	:	$R + F \longrightarrow 2R$	$k_B = A_B \exp(-\beta_B/T)$,
chain-termination	:	$R \longrightarrow P$	$k_R = 1$,

where F, R and P designate fuel, radicals and products respectively, β_I and β_B are the post-shock temperature-reduced activation energies of the initiation and branching reactions, $\beta \equiv E/R\bar{T}_N$ and T is the temperature reduced by $\bar{T}_N$. When the recombination time $\bar{t}_R$ and the recombination length, $\bar{d}_R \equiv u_N \bar{t}_R$, are used as references for time and length scales, the substantial derivatives of fuel and radical

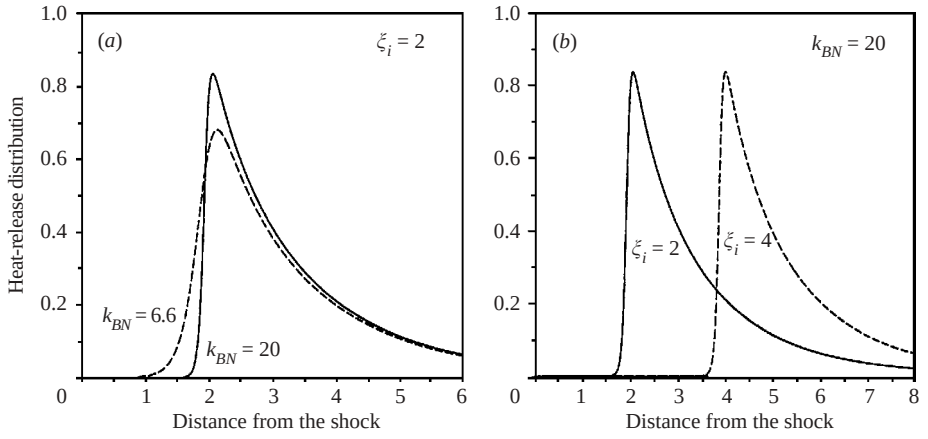

FIGURE 15. Numerical solution of the distribution of heat release rate in an unperturbed planar wave for $\gamma = 1.2$, $\beta_I = 20$, $\beta_B = 8$, $Q_0 = 10$, $f = 2$ and for different values of ξ_i and k_{NB}.

mass fractions Y_F and Y_R are given by

$$\frac{\mathrm{D}Y_F}{\mathrm{D}t} = -w_I - w_B, \qquad \frac{\mathrm{D}Y_R}{\mathrm{D}t} = w_I + w_B - w_R, \tag{5.1}$$

where $w_I = Y_F k_I$, $w_B = \rho Y_F Y_R k_B$ (ρ is the density reduced by its post-shock value), $w_R = Y_R$, and where the non-dimensional reaction rates k_I and k_B are reduced by the temperature-independent recombination rate. The governing equations are the general ones, given in Appendix C. For simplicity we assume that the heat $\hat{Q}$ is released only by the chain-termination reaction, and the notation $Q_0 \equiv \hat{Q}/\hat{R}\hat{T}_U$ will be used in the following. Realistic values of the parameters may be obtained from hydrogen–oxygen combustion (see Balakrishnan & Williams 1994 for instance), yielding $\beta_I > \beta_B \gg 1$ and $k_{IN} \ll 1 \ll k_{BN}$, where $k_{BN} \equiv A_B \exp(-\beta_B)$ and $k_{IN} \equiv A_I \exp(-\beta_I)$ are the reaction rates at the post-shock temperature $\bar{T}_N$. Typical values $\beta_I = 20$ and $\beta_B = 8$ will be kept fixed hereafter, and variations of the two other kinetics parameters A_I and A_B will be considered. Following Sanchez *et al.* (2001), the mass-weighted induction length is approximatively given by ξ_i defined as

$$\xi_i \approx \frac{1}{k_{BN}} \ln\left(\frac{k_{BN}}{k_{IN}}\right). \tag{5.2}$$

With typical values of k_{BN} and k_{IN}, ξ_i is of order unity, so that the induction time and the recombination time are of same order of magnitude. The parametric study takes a more general form when $\xi_i = O(1)$ and $k_{BN} \gg 1$ are used as independent parameters (instead of A_I and A_B), each of them having a specific effect on the distribution of heat-release rate of the unperturbed planar wave, see figure 15. For a fixed value of ξ_i, the stiffness of the thermal runaway increases with k_{BN}.

Let us consider now the effects of these two parameters upon the linear spectrum near threshold. The one-dimensional case was previously investigated by Sanchez *et al.* (2001), and the muldimensional case is presented below. In order to use (2.6), the functions $\bar{Y}_R = \bar{w}(\xi)$ and $w'_{\bar{M}_U}(\xi)$ are first computed numerically from equations (5.1) and from the isobaric conservation of energy $\mathrm{D}T/\mathrm{D}t = qY_R$, see figure 15. A typical result obtained from equation (2.6) is presented in figure 16 where $\sigma \equiv \hat{\sigma}\bar{t}_R$ and $\kappa \equiv \hat{k}\bar{d}_R/\epsilon$. Figure 16 shows the existence of two wavelength domains of unstable

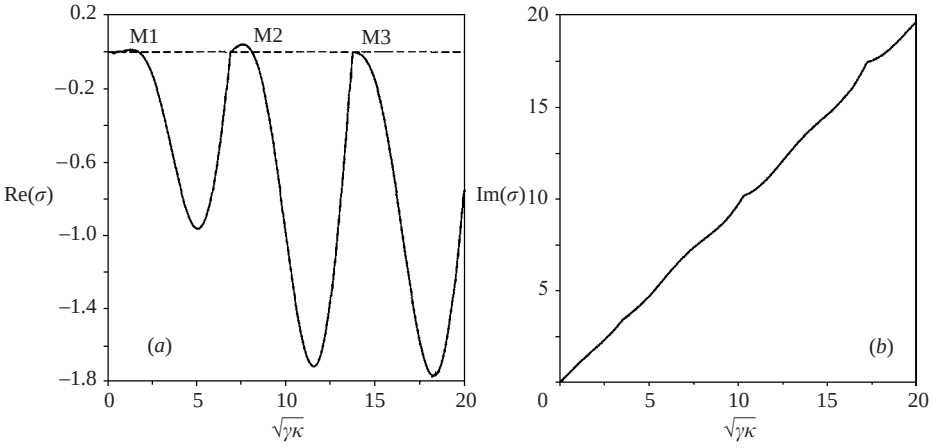

FIGURE 16. (*a*) Growth rate and (*b*) frequency obtained from equation (2.6) for the chain-branching kinetics with $\beta_I = 20$, $\beta_B = 8$, $\xi_i = 1$, $k_{NB} = 20$, $\gamma = 1.2$, $q = 0.08$ and $M_U^2 = 30$ ($f = 9.8$).

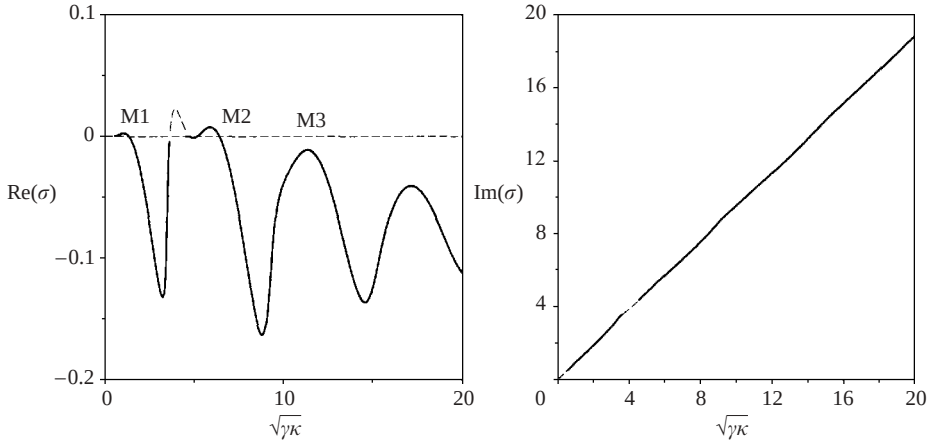

FIGURE 17. (*a*) Numerical growth rate and (*b*) frequency for the chain-branching kinetics with $\beta_I = 20$, $\beta_B = 8$, $\xi_i = 1$ and $k_{BN} = 20$, $\gamma = 1.2$, $Q_0 = 0.8$, $f = 10$ ($q = 0.04$, $M_U^2 = 21$).

disturbances. The one labelled M1 is similar to the unstable mode encountered with an Arrhenius law, see figures 3 and 4(*a*). Another one, called M2, looks similar but is shifted towards higher κ and frequencies. $\mathrm{Re}\sigma(\kappa)$ possesses two branches of solutions which are the continuations of the two branches of M1, shown in figure 3(*a*) (for clarity this is not shown in the figure 16). A series of marginally stable modes with increasing frequencies is also observed (modes M3, ...). They correspond to a repetition of the marginal mode of the stable case shown in figure 3(*a*). This may be explained from equation (2.6) as follows. According to figure 15, $\bar{w}(\xi)$ is qualitatively similar to $H(\xi - \xi_i)\exp(\xi - \xi_i)$ where $H(x)$ is the Heaviside function. Then, $w'_{\bar{M}_U}(\xi)$ contains a delta function $\delta(\xi - \xi_i)$ yielding, according to (2.8), a periodic contribution to $Z(\pm \mathrm{i}\kappa)$.

The general picture of the branches of solutions presenting both unstable and marginally stable modes being known, we turn now to numerical solutions. Since

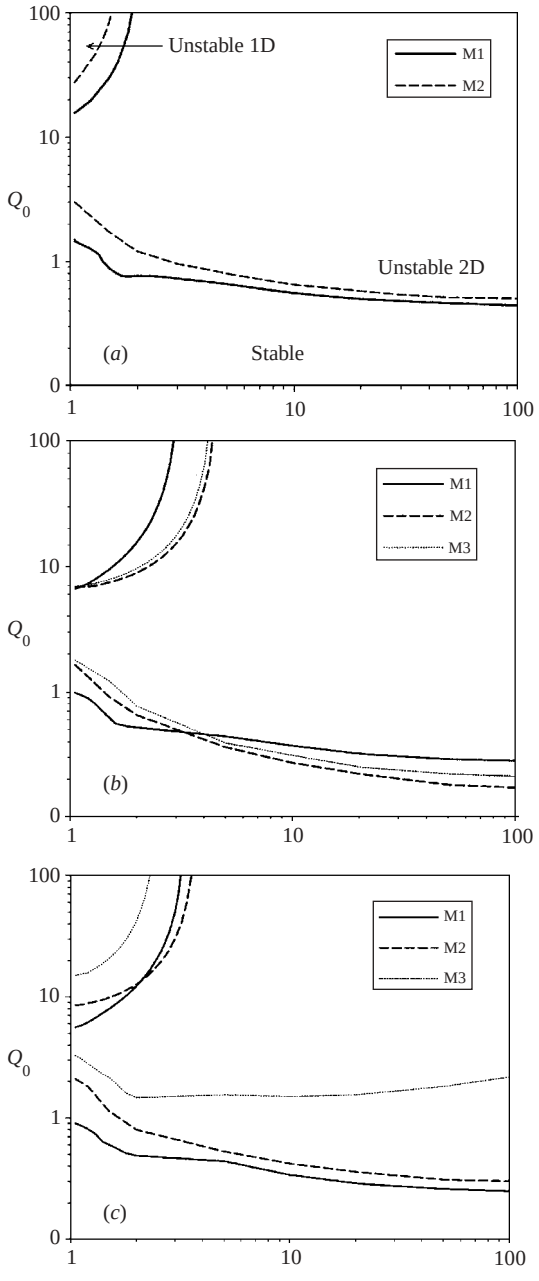

FIGURE 18. One- and two-dimensional stability limits Q_0 vs. f for modes M1 and M2 with the chain-branching kinetics for $\gamma = 1.2$, $\beta_I = 20$, $\beta_B = 8$, and (*a*) $k_{BN} = 20$, $\xi_i = 1$; (*b*) $k_{BN} = 20$, $\xi_i = 2$; (*c*) $k_{BN} = 6.6$, $\xi_i = 2$.

equation (2.6) is valid for disturbances with $\kappa = O(1)$, one cannot expect good quantitative agreement for $\kappa \gg 1$ when the wavelengths are of same order as the detonation thickness. A spectrum $\mathrm{Re}\,\sigma(\kappa)$ obtained by numerical analysis for $\gamma = 1.2$, $q = 0.04$, $\bar{M}_U^2 = 21$ ($f = 10$) is shown in figure 17. A behaviour qualitatively similar to figure 16 is observed. Instabilities appear both at a low frequency (inverse of

the transit time) and at a higher frequency (five time larger) with a wavelength five time smaller, approximatively. The marginally stable modes in figure 16 (modes M3, ...) are now stable, and their stability is reinforced on decreasing the wavelength (increasing κ). However one may expect that such modes may become unstable for particular conditions of the chemical kinetics. We now investigate this question.

The stability diagrams 'Q_0 versus f' for modes M1, M2 and M3 are shown in figure 18(*a–c*), exhibiting clearly the effects of the the two parameters ξ_i and k_{BN}. The multidimensional instability is observed at a critical Q_0 smaller than that for the one-dimensional instability (the linear growth rate is strictly positive at $\kappa = 0$ in regions labelled 'unstable 1D' and negative elsewhere). In figure 18(*a*) where $k_{BN} = 20$ and $\xi_i = 1$, the mode M1 is unstable before M2, irrespective of the values of the overdrive factor f. As shown in figure 18(*b*), this is no longer the case for sufficiently large overdrive when the mass-weighted induction length is increased, $\xi_i = 2$: M2 and M3 now become unstable before M1 when $f > 3$. Under such conditions, small cells pulsating with a high frequency appear first! This is a consequence of the multiple-step chemistry involving a distribution of heat-release rate whose variations are shown in figure 15. However, as shown in figure 18(*c*) where $\xi_i = 2$ and $k_{BN} = 6.6$, a decrease of k_{BN} returns to a situation similar to figure 18(*a*) where the mode M1 becomes unstable before M2 and M3 for all f.

Concerning the mode M1, a comparison of the numerical results with (2.6) leads to the same conclusions as in the preceding section for an Arrhenius law. More particularly the same qualitative change of the branch of solution that bifurcates, mentioned at the end of § 4 and shown in figure 14, is also observed for small overdrive when approaching C-J conditions.

6. Conclusions

The linear spectrum for transverse instability of a gaseous detonation involves a complex set of branches of modes. A detailed study of this spectrum near the instability threshold (a first step toward a weakly nonlinear analysis of cellular structures) has been carried out for both a one-step Arrhenius law and multiple-step chemistry, combining numerical and analytical results.

A general finding for multiple-step chemistry having an induction time of the same order of magnitude as the recombination time (see figure 15), is that there are transverse oscillatory instabilities for different domains of wavelengths and frequencies which are separated by domains where the wave is linearly stable (see figure 17). Increasing either the induction time (compared to the recombination time) or the stiffness of the thermal runaway leads to instability to transverse disturbances with small wavelengths and high frequencies, coexisting in general with unstable disturbances with long wavelengths (much larger than the detonation thickness) and low frequencies (of same order as the inverse of the transit time). This could be related to two-level cellular structure, with a sub-structure contained in a main structure, observed, for example, in some experiments with gaseous nitromethane, see Presles *et al.* (1996). According to our numerical analysis, instability may well appear first at small wavelength and high frequency in some conditions for $f > 3$, see figure 18(*b*). Instabilities at long wavelengths and low frequencies are similar to those observed with a one-step Arrhenius law near threshold.

The distinguished limit (2.2) provides analytical results with a clear physical meaning, particularly helpful for detonations sustained by complex chemistry. A systematic comparison with numerical results for the so-called 'hydrodynamical

instability' (one-step Arrhenius kinetics with a zero activation energy) shows that these results are accurate when $\gamma \leqslant 1.3$ down to moderate overdrive, $f \approx 3$. They are qualitatively satisfactory even below $f = 3$ and, in any case, are much better than those obtained with a simple expansion for small heat release, which is accurate for the stability limits only at large overdrive. The conclusions are similar for the low-frequency mode of a detonation supported by a multiple-step chemistry.

The physical mechanisms responsible for the cellular structures are clearly exhibited for large and moderate overdrive within the framework of a Newtonian approximation because the compressible effects and the isobaric gas expansion by heat release become distinguishable. The main advantage of the perturbative analysis based on the distinguished limit (2.2) is to take into account accurately the compressibility effects at the first order, near the stability limits where the heat release devided by the post-shock enthalpy, $\hat{Q}/c_p\bar{T}_N$, becomes as small as $(\gamma - 1)$, so that $\hat{Q}/R\bar{T}_N$ is of order unity. However near the C-J regime, $f < 1.3$, the compressibility effects become dominant near threshold, new behaviours are observed in the numerical spectrum, and a different theoretical analysis is required, see Clavin & Williams (2002).

Appendix A. Outline of the analysis of Clavin & He (2001)

Non-dimensional variables are $u = \hat{u}/\bar{u}_N$, $\boldsymbol{v} = \epsilon\hat{\boldsymbol{v}}/\bar{u}_N$, $p = \hat{p}/\bar{p}_N$, $T = \hat{T}/\bar{T}_N$ and $\alpha = \hat{\alpha}/\bar{d}$, where $\hat{u}$, $\hat{\boldsymbol{v}}$, $\hat{p}$ and $\hat{T}$ denote the longitudinal and transverse velocities, the pressure and the temperature (overbars are for the unperturbed state and subscript N denotes the post-shock state). Scaling for $\hat{\boldsymbol{v}}$ results from the large jump of the flow velocity across the wrinkled shock due to a large density jump, $\bar{\rho}_N/\rho_U \approx 1/\epsilon^2$, where ρ_U denotes the initial density of the gas. Boundary conditions for the linear solution of the reactive Euler equation are the Rankine–Hugoniot shock conditions at $\xi = 0$, and when the piston is at infinity in the burned gas, a boundedness condition for the acoustic perturbations at $\xi \to \infty$. For linearly unstable modes this last condition is equivalent to a radiation condition. The shock conditions, see equations (C5)–(C9) in Appendix C, take the form

$$\delta u_N \approx \left[1 + \frac{1}{M_U^2} - \frac{(\gamma-1)}{2}\right]\dot{\alpha}_\tau, \qquad \boldsymbol{\delta v}_N \approx \left[1 - \frac{1}{M_U^2}\right]\nabla\alpha, \tag{A 1}$$

$$\delta p_N \approx -2\epsilon^2\dot{\alpha}_\tau, \qquad \delta T_N \approx -(\gamma-1)\dot{\alpha}_\tau, \tag{A 2}$$

valid in the linear aproximation up to $O(\epsilon^2)$, and where $\dot{\alpha}_\tau \equiv \partial\alpha/\partial\tau$, and ∇ denotes the gradient in the transverse directions. In the same approximation and after elimination of the density, the linear reactive Euler equations take a simple form when the mass-weigthed coordinate ξ is used, see Clavin *et al.* 1997 and Clavin & He 2001:

$$\epsilon^2\left[\left(\frac{\partial}{\partial\tau} + \frac{\partial}{\partial\xi}\right)\delta u - \delta v\frac{d\bar{u}}{d\xi}\right] = -\frac{\partial\delta p}{\partial\xi}, \tag{A 3}$$

$$\left(\frac{\partial}{\partial\tau} + \frac{\partial}{\partial\xi}\right)(\nabla\cdot\boldsymbol{\delta v}) = -\bar{u}\nabla^2\delta p, \tag{A 4}$$

$$\frac{1}{\gamma}\frac{\bar{u}}{\bar{p}}\left(\frac{\partial}{\partial\tau} + \frac{\partial}{\partial\xi}\right)\delta p + \frac{\partial}{\partial\xi}(\delta u + \bar{u}\delta v) = q(\delta w + \delta v\bar{w}), \tag{A 5}$$

where $\delta v(\xi, \boldsymbol{\eta}, \tau) \equiv \int_0^\xi \nabla\cdot\boldsymbol{\delta v}\,\mathrm{d}\xi'$. In the burned gas the reaction source terms $\bar{w}$ and δw vanish, the unperturbed solution is uniform, and an exact solution to the linear equations (A3)–(A5) is easily obtained. The solution is a superposition of a

sound wave (superscript a) and an isobaric entropy–vorticity wave (superscript i) $\delta u = \delta u^{(a)} + \delta u^{(i)}$, $\boldsymbol{\delta v} = \boldsymbol{\delta v}^{(a)} + \boldsymbol{\delta v}^{(i)}$, $\delta p = \delta p^{(a)}$ and $\delta p^{(i)} = 0$. Written in Fourier representation with the notation of (2.3), $\delta p = \delta p^*(\xi)\exp(s\tau + \mathrm{i}\boldsymbol{\kappa}\cdot\boldsymbol{\eta})$, the d'Alembert equation yields

$$\left\{\frac{1}{\gamma}\frac{\bar{u}_B}{\bar{p}_B}\left(\frac{\mathrm{d}}{\mathrm{d}\xi}+s\right)^2-\frac{1}{\epsilon^2}\frac{\mathrm{d}^2}{\mathrm{d}\xi^2}+\bar{u}_B^2\kappa^2\right\}\delta p^*(\xi)=0. \tag{A 6}$$

The solution $\delta p^*(x) = \delta p_B^* \exp(\mathrm{i}l\xi)$ of (A 6) may be written in a convenient form in terms of $\varepsilon^2 \equiv (\bar{u}_B/\gamma\bar{p}_B)\epsilon^2$ and $\varkappa^2 \equiv (\gamma\bar{u}_B\bar{p}_B)\kappa^2$,

$$\mathrm{i}l=\frac{\varepsilon^2 s \pm \varepsilon\sqrt{s^2+\varkappa^2-\varepsilon^2\varkappa^2}}{1-\varepsilon^2}. \tag{A 7}$$

When $(s^2+\varkappa^2)$ is different from zero and of order unity, $\mathrm{i}l$ is of order ε in the limit $\epsilon \to 0$, $\mathrm{i}l = \pm\varepsilon\sqrt{s^2+\varkappa^2} + O(\varepsilon^2)$. The situation is different in the limit (2.2) where $q = O(\epsilon^2)$, $\bar{p}_B = 1 + O(\epsilon^4)$ and $\bar{u}_B = 1 + q + O(\epsilon^4)$. As we will see, s and $\varkappa$ are of order unity but $(s^2+\varkappa^2)$ is of order ε^2, see equation (A 11) below, leading to $\mathrm{i}l = O(\varepsilon^2)$, $\mathrm{i}l = \epsilon^2\mathrm{i}l_2$ with $\mathrm{i}l_2 = O(1)$. The longitudinal length scale of the pressure is then larger than the detonation thickness by a factor $1/\epsilon^2$, expressing that the sound waves propagate in the burned gas in a direction quasi-parallel to the unperturbed shock. Anticipating that the same scaling is also valid throughout the detonation structure, see discussion below equations (A 14) and (A 16), we find that the leading-order pressure may be expressed in terms of the post-shock fluctuations (A 2),

$$\delta p^*(\epsilon^2\xi) = -2\epsilon^2 s\alpha^* \exp(\mathrm{i}\epsilon^2 l_2\xi) + O(\epsilon^4). \tag{A 8}$$

The entropy–vorticity wave in the burned gas is the solution of equations (A 3)–(A 5) with $\bar{w} = 0$, $\delta w = 0$, $\bar{u} = \bar{u}_B = 1 + q + O(\epsilon^4)$ and $\delta p = 0$,

$$\left(\frac{\partial}{\partial\tau}+\frac{\partial}{\partial\xi}\right)\delta u^{(i)}=0,\quad \left(\frac{\partial}{\partial\tau}+\frac{\partial}{\partial\xi}\right)\boldsymbol{\delta v}^{(i)}=0,\quad \frac{\partial}{\partial\xi}\delta u^{(i)}+\bar{u}_B\boldsymbol{\nabla}\cdot\boldsymbol{\delta v}^{(i)}=0. \tag{A 9}$$

According to equation (A 8), the amplitude of the acoustic flow is small, of order ϵ^2 and the leading-order flow field is fully controlled by the entropy–vorticity wave, (A 9) yielding, when the boundary conditions (A 1) are used,

$$\delta u_0^{(i)} = \frac{\partial\alpha}{\partial\tau}(\tau-\xi,\eta),\qquad \boldsymbol{\delta v}_0^{(i)} = \boldsymbol{\nabla}\alpha(\tau-\xi,\eta). \tag{A 10}$$

The continuity equation, the third equation in (A 9), is $\partial\delta u_0^{(i)}/\partial\xi + \boldsymbol{\nabla}\cdot\boldsymbol{\delta v}_0^{(i)} = 0$, yielding the wave equation (2.5) for the evolution of the front,

$$s_0 = \pm\mathrm{i}\kappa. \tag{A 11}$$

The leading-order frequency of the oscillatory modes is thus given by the isobaric entropy–vorticity wave of a strong inert shock. With the notation of (2.4), and introducing $q_2 = O(1)$, $q \equiv \epsilon^2 q_2$, one then obtains from (A 7),

$$\mathrm{i}l_2 = s_0 - \left[2s_0 s_2 + \left(\frac{\gamma-1}{\epsilon^2}+q_2-1\right)\kappa^2\right]^{1/2} + O(\epsilon^2), \tag{A 12}$$

where by definition $\mathrm{Re}[\ldots]^{1/2} > 0$, and the minus sign in front of $[\ldots]^{1/2}$ is chosen in order to satisfy the boundedness of the acoustic waves at $\xi \to +\infty$, $\mathrm{Re}(\mathrm{i}l_2) < 0$. The presence of q_2 in the square root points out the difference from a simple expansion

for small heat release. This comes from equation (A 7) where $(s^2+\varkappa^2)=O(\epsilon^2)$ and from the expressions for ε and $\varkappa$ with $\bar{u}_B=1+q+O(\epsilon^4)$.

The flow velocity in the burned gas is then obtained from (A 1)–(A 5) and (A 8) in the form

$$\left.\begin{aligned}\delta u^{*(i)}&=\left(s_0+\epsilon^2\delta u^{*(i)}_{B2}\right)\alpha^*\exp(-s\xi), &\quad \boldsymbol{\nabla\cdot\delta v}^{*(i)}&=\left(-\kappa^2+\epsilon^2\boldsymbol{\nabla\cdot\delta v}^{*(i)}_{B2}\right)\alpha^*\exp(-s\xi),\\ \delta u^{*(a)}&=2\epsilon^2 \mathrm{i} l_2\alpha^*\exp(\mathrm{i}\epsilon^2 l_2\xi), &\quad \boldsymbol{\nabla\cdot\delta v}^{*(a)}&=-2\epsilon^2\kappa^2\alpha^*\exp(\mathrm{i}\epsilon^2 l_2\xi),\end{aligned}\right\} \tag{A 13}$$

valid up to order ϵ^2, where $\delta u^{*(i)}_{B2}$ and $\boldsymbol{\nabla\cdot\delta v}^{*(i)}_{B2}$ are constants of integration that are linked together by the continuity equation, the third equation in (A 9). The complete flow field throughout the detonation structure is determined by introducing the splitting

$$\delta u^*\equiv\delta U^{*(i)}(\xi)+\delta u^{*(a)}(\epsilon^2\xi),\quad \boldsymbol{\delta v}^*\equiv\boldsymbol{\delta V}^{*(i)}(\xi)+\boldsymbol{\delta v}^{*(a)}(\epsilon^2\xi). \tag{A 14}$$

According to (A 8), the longitudinal pressure gradient is of order ϵ^4 in the burned gas. Anticipating that this is also true everywhere behind the shock, we conclude that the pressure variation throughout the reaction zone is smaller than the post-shock fluctuations, and the pressure is quasi-uniform throughout the detonation structure. After subtracting out the acoustics, equation (A 5) leads to the isobaric approximation of low Mach number, the divergence of the flow $(\delta U^{*(i)};\boldsymbol{\delta V}^{*(i)})$ is balanced by the rate of gas expansion due to heat release qw,

$$\mathrm{d}\delta U^{*(i)}/\mathrm{d}\xi+\bar{u}\boldsymbol{\nabla\cdot\delta V}^{*(i)}\approx q\delta w, \tag{A 15}$$

yielding

$$\frac{\mathrm{d}}{\mathrm{d}\xi}\left[\delta U^{*(i)}+\bar{u}(\xi)\int_0^\xi\left(\boldsymbol{\nabla\cdot\delta V}^{(i)}\right)^*\mathrm{d}\xi'\right]\approx q\left(\delta w^*+\delta v_0^{*(i)}\bar{w}\right), \tag{A 16}$$

where the relation $\mathrm{d}\bar{u}/\mathrm{d}\xi=q\bar{w}$ has been used. Equation (A 16) is valid up to order $\varepsilon^2\delta\alpha$. The post-shock fluctuations of pressure (A 2) are fully absorbed by the sound wave in the burned gas, and the longitudinal variations of the pressure through the detonation structure are of order ϵ^4. Then, the first two orders of the quantity $\boldsymbol{\nabla\cdot\delta V}^{(i)}$ are, according to (A 4), simply advected by the flow field from the shock, $(\partial/\partial\tau+\partial/\partial\xi)\boldsymbol{\nabla\cdot\delta V}^{(i)}=O(\epsilon^4)$, leading to

$$\boldsymbol{\nabla\cdot\delta V}^{*(i)}=\left[-1+\epsilon^2\left(2+\frac{1}{\epsilon^2M_U^2}\right)\right]\kappa^2\alpha^*\exp(-s\xi)+O(\epsilon^4), \tag{A 17}$$

where the boundary condition for $\boldsymbol{\nabla\cdot\delta V}^{*(i)}$ at $\xi=0$ given by (A 1) and (A 13) has been used. The boundary condition $\delta U^{*(i)}(\xi=0)$ is obtained in the same way, and a forward integration of equation (A 16) with respect to ξ from the shock $\xi=0$ then yields

$$\begin{aligned}\delta U^{*(i)}(\xi)-\left[1+\frac{1}{M_U^2}-\frac{\gamma-1}{2}\right]s\alpha^*+2\epsilon^2\mathrm{i}l_2\alpha^*+\bar{u}(\xi)\int_0^\xi\left(\boldsymbol{\nabla\cdot\delta V}^{(i)}\right)^*\mathrm{d}\xi'\\ =q\int_0^\xi\left[\delta w^*(\xi')+\delta v_0^{*(i)}(\xi')\bar{w}(\xi')\right]\mathrm{d}\xi'+O(\epsilon^4),\end{aligned} \tag{A 18}$$

into which equation (A 17) and the expansion (2.4) have to be introduced. The expression $\delta U^{*(i)}(\xi)$ in equation (A 18) contains two kinds of terms at the end of the reaction when $\xi\gg1$, $\delta w^*(\xi')=0$, $\bar{w}(\xi')=0$: the first do not vary with ξ while

the second do depend on ξ through $\exp(-s\xi)$ exhibiting the same fast oscillations $\exp(\pm \mathrm{i}\kappa\xi)$ damped on a longer length scale as for $\delta u^{*(i)}$ in (A 13), $\exp(-\epsilon^2 s_2 \xi)$ with $\mathrm{Re}\, s_2 > 0$ for unstable cases. By definition, the limit of $\delta U^{*(i)}$ when $\xi \gg 1$ must be equal to $\delta u^{*(i)}$. The matching condition then requires that the sum of all constant terms must be set to zero, yielding

$$2\epsilon^2(\mathrm{i}l_2) - s\left[1 + \frac{1}{M_U^2} - \frac{\gamma-1}{2}\right] + (1+q)\left[-1 + \epsilon^2\left(2 + \frac{1}{\epsilon^2 \bar{M}_U^2}\right)\right]\frac{\kappa^2}{s}$$

$$= \frac{q}{\alpha^*}\int_0^\infty \left[\delta w^*(\xi) + \delta v_0^{*(i)}(\xi)\bar{w}^*(\xi)\right]\mathrm{d}\xi + O(\epsilon^4). \quad \text{(A 19)}$$

Matching the oscillatory terms gives the constant of integration $\delta u_{B2}^{*(i)}$ in (A 13). Compressional heating being negligible at the leading order, the integral on the right-hand side of equation (A 19) is computed from the equations for temperature and chemical species which form in the quasi-isobaric approximation a closed set of equations whose solution expresses the fluctuations of the distribution of heat-release rate in terms of the history of the fluctuations of front position and velocity, yielding, see Clavin *et al.* (1997),

$$\frac{\partial}{\partial\tau}\int_0^\infty \left[\delta w + \delta v_0^{(i)}\bar{w}\right]\mathrm{d}\xi = \nabla^2\alpha(\tau) - \int_0^\infty \bar{w}'_{\bar{M}_U}(\xi)\frac{\partial^2}{\partial\tau^2}\alpha(\tau-\xi)\,\mathrm{d}\xi$$

$$- \int_0^\infty \bar{w}(\xi)\left[1 + \xi\frac{\partial}{\partial\tau}\right]\nabla^2\alpha(\tau-\xi)\,\mathrm{d}\xi + O(\epsilon^2), \quad \text{(A 20)}$$

which may be written at the leading order and using the notation of (2.8) as

$$\frac{1}{\alpha^*}\int_0^\infty \left[\delta w^* + \delta v_0^{*(i)}\bar{w}^*\right]\mathrm{d}\xi = \frac{\kappa^2}{s}[-1 + Z(s_0)] + O(\epsilon^2). \quad \text{(A 21)}$$

An equation for the linear growth rate s_2 is obtained from (A 19) and (A 21),

$$-\frac{s_0}{\kappa}\sqrt{2\frac{s_0 s_2}{\kappa^2} + \frac{\gamma-1}{\epsilon^2} + q_2 - 1} - \frac{s_0 s_2}{\kappa^2} + 1 - \frac{3(\gamma-1)}{4\epsilon^2} = \frac{q_2}{2}Z(s_0), \quad \text{(A 22)}$$

where, by definition $\mathrm{Re}(\sqrt{\ldots}) > 0$. The two roots of the quadratic equation obtained from (A 22) are

$$s_2 = s_0\left[\frac{3(\gamma-1)}{4\epsilon^2} + \frac{q_2}{2}Z\right] \pm s_0\sqrt{\frac{\gamma-1}{2\epsilon^2} + q_2(Z-1)}. \quad \text{(A 23)}$$

The solution of (A 22) must satisfy the relation $\mathrm{Re}[s_2 - s_0(q/2)Z] \leqslant 0 \Rightarrow \mathrm{Re}[\pm s_0\sqrt{\ldots}] < 0$. According to (A 23) and using the relation $(\epsilon^2/q)\sqrt{(\gamma-1)/2\epsilon^2} = (1/Q)\sqrt{2\epsilon^2/(\gamma-1)}$ with $2\epsilon^2/(\gamma-1) \approx [1+2/(\gamma-1)\bar{M}_U^2]$, this solution yields equation (2.6). The acoustic fields are then obtained from (A 12), (A 13) and (A 23),

$$\mathrm{i}\epsilon^2 l_2 = s_0\epsilon^2\left[2 \pm \sqrt{\frac{\gamma-1}{2\epsilon^2}}\sqrt{1 + Q(Z-1)}\right], \quad \text{(A 24)}$$

where $s_0 = \pm\mathrm{i}\kappa$ and the $\pm$ sign inside the brackets of (A 24) has to be choosen as above, $\mathrm{Re}[\pm s_0\sqrt{\ldots}] < 0 \Rightarrow \mathrm{Re}(\mathrm{i}l_2) \leqslant 0$. According to (A 24), the square-root term in equation (2.6) describes a damping by coupling sound waves with heat release. According to equations (A 18) and (A 22), this term comes from the boundary value $\delta u^{*(a)}(\xi = 0)$ and thus describes what is called in the thermo-acoustic literature a 'velocity coupling',

while, according to equations (A 19)–(A 23), the first term on the right-hand side of equation (2.6) describes the effect of a quasi-isobaric expansion due to heat release. This last mechanism could be considered in gaseous detonations as similar to the 'Darrieus–Landau' instability in flames, but with the drastic difference that it results from a modification to the inner structure of the wave.

The form of the square-root term in equation (A 24) illustrates that the sound waves cannot be accurately captured by a simple expansion in powers of the heat release when Q is not small, i.e. when q is not much smaller than $(\gamma - 1)$. This is precisely the case at the instability threshold for moderate and small overdrive, see figures 8(a), 10(a), 12(a) and 14.

Appendix B. Time and length scales

For an Arrhenius law $\hat{w} = \hat{B}(1-\lambda)\exp(-\hat{E}/R\hat{T})$, time and length scales in Clavin & He (2001) are $\bar{t}_N = \exp(\beta)/\hat{B}$ and $\bar{d}_N = \bar{u}_N \bar{t}_N$, where $\beta = \hat{E}/R\bar{T}_N$. Time and length scales in Short & Stewart (1999) are

$$\bar{t}_{1/2} \equiv \frac{\bar{d}_{1/2}}{\bar{c}_N}, \qquad \bar{d}_{1/2} \equiv \frac{1}{\hat{B}} \int_0^{1/2} \frac{\bar{\hat{u}}}{(1-\lambda)} \exp\left(\frac{\hat{E}}{R\bar{\hat{T}}}\right) \mathrm{d}\lambda,$$

where $\bar{c}_N$ is the post-shock sound speed of the unperturbed solution. The relation between the two scales is obtained by computing the following integral:

$$I = \bar{M}_N \int_0^{1/2} \frac{\bar{u}}{(1-\lambda)} \exp\left(\beta \frac{1-\bar{T}}{\bar{T}}\right) \mathrm{d}\lambda. \tag{B 1}$$

At the leading order in the limit (3.3), we obtain $\bar{u} \approx 1$, $\bar{T} \approx 1$ and therefore $I \approx \bar{M}_N \ln(2)$.

Appendix C. Numerical method

C.1. *Equations*

The general equations are the Euler reactive equations that describe the flow behind the leading shock. The gas is considered to be ideal with constant specific heats. A coordinate system is adopted in which the planar shock preceding the unperturbed detonation is located at the plane $\hat{x} = 0$, with the unshocked gas occupying the region $\hat{x} < 0$. With $\hat{\nabla}$ denoting the transverse gradient operator in this coordinate system, the substantial derivative becomes $\mathrm{D}/\mathrm{D}\hat{t} = \partial/\partial\hat{t} + \hat{u}\partial/\partial\hat{x} + \hat{\nabla}\cdot\hat{\boldsymbol{v}}$. The equations for conservation of mass, longitudinal and transverse momentum, energy and species then become, respectively,

$$\frac{1}{\hat{\rho}}\frac{\mathrm{D}\hat{\rho}}{\mathrm{D}\hat{t}} + \frac{\partial\hat{u}}{\partial\hat{x}} + \hat{\nabla}\cdot\hat{\boldsymbol{v}} = 0, \tag{C 1}$$

$$\hat{\rho}\frac{\mathrm{D}\hat{u}}{\mathrm{D}\hat{t}} = -\frac{\partial\hat{p}}{\partial\hat{x}}, \qquad \hat{\rho}\frac{\mathrm{D}\hat{\boldsymbol{v}}}{\mathrm{D}\hat{t}} = -\hat{\nabla}\hat{p}, \tag{C 2}$$

$$\frac{1}{\gamma}\frac{1}{\hat{p}}\frac{\mathrm{D}\hat{p}}{\mathrm{D}\hat{t}} - \frac{1}{\hat{\rho}}\frac{\mathrm{D}\hat{\rho}}{\mathrm{D}\hat{t}} = \frac{\hat{Q}}{c_p\hat{T}}\hat{w}, \tag{C 3}$$

$$\frac{\mathrm{D}Y_i}{\mathrm{D}\hat{t}} = \hat{w}_i, \qquad i = 1\ldots N, \tag{C 4}$$

where Y_i denotes the mass fraction of chemical species i in the N-component gas mixture, $\hat{\rho}\hat{w}_i$ the mass rate of production of chemical species i per unit volume and $\hat{\rho}\hat{Q}\hat{w}$ the rate of energy release per unit volume by the chemical reactions, $\hat{Q}$ representing the total amount of energy released per unit mass of the gas mixture. Pressure, temperature and density are related by the ideal gas law, $\hat{p}/\hat{\rho} = R\hat{T}$ $(R = c_p - c_v)$.

C.2. *Boundary conditions*

Linearized boundary conditions at the shock are given by

$$\frac{\delta\hat{\rho}_N}{\bar{\rho}_N} = -\frac{4}{(\gamma+1)\bar{M}_U^2}\frac{1}{\bar{u}_N}\frac{\partial\hat{\alpha}}{\partial\hat{t}}, \tag{C 5}$$

$$\frac{\delta\hat{p}_N}{\bar{p}_N} = \frac{-4\gamma\bar{M}_N^2}{\gamma+1}\frac{1}{\bar{u}_N}\frac{\partial\hat{\alpha}}{\partial\hat{t}}, \tag{C 6}$$

$$\frac{\delta\hat{T}_N}{\bar{T}_N} = -2\frac{\gamma-1}{\gamma+1}\frac{1}{\bar{u}_N}\frac{\partial\hat{\alpha}}{\partial\hat{t}}, \tag{C 7}$$

$$\frac{\delta\hat{u}_N}{\bar{u}_N} = 2\frac{\bar{M}_U^2+1}{(\gamma+1)\bar{M}_U^2}\frac{1}{\bar{u}_N}\frac{\partial\hat{\alpha}}{\partial\hat{t}}, \tag{C 8}$$

$$\frac{\delta\hat{\boldsymbol{v}}_N}{\bar{u}_N} = 2\frac{\bar{M}_U^2-1}{(\gamma-1)\bar{M}_U^2+2}(\hat{\nabla}\hat{\alpha}). \tag{C 9}$$

A shooting method is applied by using the boundary conditions (C5)–(C9) plus a compatibility condition in the burned gases expressing that the flow of the entropy–vorticity wave must be divergence free. Written in the notation of Clavin *et al.* (1997), $\delta\hat{\phi}(\hat{x},\hat{\boldsymbol{y}},\hat{t}) = \delta\hat{\phi}^*(\hat{x})_{\hat{\boldsymbol{k}},\hat{\sigma}}\exp(\hat{\sigma}\hat{t} + \mathrm{i}\hat{\boldsymbol{k}}\cdot\hat{\boldsymbol{y}})$, this compatibility condition is

$$\pm\sqrt{1+S^2}\frac{\delta\hat{p}_B^*}{\bar{\rho}_B\bar{c}_B\bar{u}_B} + S\frac{\delta\hat{u}_B^*}{\bar{u}_B} - \frac{\mathrm{i}\hat{\boldsymbol{k}}\cdot\delta\hat{\boldsymbol{v}}_B^*}{\hat{k}\bar{u}_B}\frac{\bar{M}_B}{\sqrt{1-\bar{M}_B^2}} = 0, \tag{C 10}$$

where $S \equiv \hat{\sigma}/(\bar{c}_B\hat{k}\sqrt{1-\bar{M}_B^2})$, $\bar{c}_B$ is the sound speed in the burned gas, and the sign $(\pm)$ must be chosen to enforce boundedness of acoustic waves for $\hat{x} \to +\infty$. We show below that this condition corresponds to a radiation condition for an unstable perturbation $(\mathrm{Re}(\hat{\sigma}) > 0)$.

C.3. *Discussion of the rear boundary condition*

By using the notation $\hat{p}_B(\hat{x},\hat{\boldsymbol{y}},\hat{t}) \propto \exp(\mathrm{i}\hat{l}\hat{x} + \mathrm{i}\hat{\boldsymbol{k}}\cdot\hat{\boldsymbol{y}} + \hat{\sigma}\hat{t})$, where $\hat{\sigma} = \mathrm{Re}(\hat{\sigma}) + \mathrm{i}\hat{\omega}$, $\hat{\omega} > 0$ ($\hat{l}$ is a complex number and $\hat{\boldsymbol{k}}$ is real), the longitudinal component of the propagation velocity (relative to the shock) of a sound wave in the burned gas is

$$\hat{u}_g = \bar{\hat{u}}_B - \bar{c}_B\frac{\mathrm{Re}(\hat{l})}{\sqrt{[\mathrm{Re}(\hat{l})]^2 + \hat{k}^2}}, \tag{C 11}$$

where $\bar{\hat{u}}_B$ is the flow velocity in the burned gas of the unperturbed solution. The longitudinal wave vector $\hat{l}$ is given by (A 24) with $s_0 = +\mathrm{i}\kappa$, $\kappa > 0$, yielding

$$u_g \equiv \frac{\hat{u}_g}{\bar{u}_N} = -\left[1 \pm \left(\frac{\gamma-1}{2\epsilon^2}\right)^{1/2}\mathrm{Re}\sqrt{1+Q[Z(+\mathrm{i}\kappa)-1]}\right] + O(\epsilon^2), \tag{C 12}$$

where by definition $\mathrm{Re}(\sqrt{\ldots}) > 0$, and the $\pm$ sign must be choosen to satisfy a boundedness condition for sound waves in the burned gas, $\pm\mathrm{Im}\sqrt{1+Q[Z(+\mathrm{i}\kappa)-1]} > 0$.

Numerical results show that the right-hand side of (C 12) is systematically positive for an unstable situation, $\mathrm{Re}(s) > 0$ where $\mathrm{Re}(s)$ is given in (2.6). The acoustic waves associated with unstable modes of a gaseous detonation are thus outgoing, $u_g > 0$, while they are incoming for the neutral modes of a pure shock, $u_g < 0$, see equation (C 12) with $Q = 0$ and where $(\gamma - 1)/2\epsilon^2 < 1$. This can be easily shown in the limit (3.3) for an 'hydrodynamic instability', $\beta(\gamma - 1) << 1$; the general case is more tedious to carry out. Equations (3.1) and (C 12) yield

$$u_g = \left[-\frac{1}{(\gamma - 1)M_U^2} - \frac{Q}{2}\left(\frac{\kappa}{\kappa^2 + 1}\right)^2 (\kappa^2 - 1) \right] + \text{h.o.t.} \qquad \text{(C 13)}$$

Except for a positive factor, this expression is the same as (3.2), showing that the sound waves are outgoing in unstable cases.

REFERENCES

Balakrishnan, G. & Williams, F. A. 1994 Turbulent combustion regimes for hypersonic propulsion employing hydrogen-air diffusion flames. *J. Prop. Power* **10**, 434–437.

Clavin, P. & Denet, B. 2002 Diamond patterns in cellular detonations of overdriven detonations. *Phys. Rev. Lett.* **88**(4), 44502–1.

Clavin, P. & He, L. 1996 Stability and nonlinear dynamics of one-dimensional overdriven detonations in gases. *J. Fluid Mech.* **306**, 353–378.

Clavin, P. & He, L. 2001 Theory of cellular detonations in gases. Part 1. stability limits at strong overdrive. *C. R. Acad. Sci. Paris* **329**(IIb), 463–471.

Clavin, P., He, L. & Williams, F. 1997 Multidimensional stability analysis of overdriven gaseous detonations. *Phys. Fluids* **9**, 3764–3785.

Clavin, P. & Williams, F. A. 2002 Dynamics of planar gaseous detonations near chapman-jouguet conditions for small heat release. *Combust. Theory Modelling* **6**, 127–139.

D'yakov, S. 1954 The stability of shock waves : investigation of the problem of the stability of shock waves in arbitrary media. *Zh. Eksp. Teor. Fiz.* **27**, 288.

Erpenbeck, J. 1964 Stability of idealized one-reaction detonations. *Phys. Fluids* **7**, 684–696.

Erpenbeck, J. 1965 Stability of idealized one-reaction detonations: Zero activation energy. *Phys. Fluids* **8**, 1192–1193.

Kontorovich, V. 1957 Concerning the stability of shock waves. *Zh. Eksp. Teor. Fiz.* **33**, 1525.

Lee, H. & Stewart, D. 1990 Calculation of linear detonation instability: one-dimensional instability of plane detonation. *J. Fluid Mech.* **216**, 103–132.

Presles, H., Desbordes, D., Guirard, M. & Guerraud, C. 1996 Gaseous nitromethane and nitromethane-oxygen mixtures: a new detonation structure. *Shock Wave* **6**, 111–114.

Sanchez, A. L., Carretero, M., Clavin, P. & Williams, F. A. 2001 One-dimensional overdriven detonations with branched-chain kinetics. *Phys. Fluids* **13**, 776–792.

Short, M. & Dold, J. W. 1996 Linear stability of a detonation wave with a model three-step chain-branching reaction. *Math. Comput. Modelling* **24**(8), 115–123.

Short, M. & Stewart, D. 1998 Cellular detonation stability. Part 1. a normal-mode linear analysis. *J. Fluid Mech.* **368**, 229–262.

Short, M. & Stewart, D. 1999 The multi-dimensional stability of weak-heat-release detonations. *J. Fluid Mech.* **382**, 103–135.